Atmos. Chem. Phys. Discuss., 9, 15769–15825, 2009
www.atmos-chem-phys-discuss.net/9/15769/2009/

Atmospheric Chemistry and Physics Discussions

This discussion paper is/has been under review for the journal *Atmospheric Chemistry and Physics (ACP)*. Please refer to the corresponding final paper in *ACP* if available.

Evaluation of black carbon estimations in global aerosol models

D. Koch[1,2], M. Schulz[3], S. Kinne[4], T. C. Bond[6], Y. Balkanski[3], S. Bauer[1,2], T. Berntsen[13], O. Boucher[14], M. Chin[15], A. Clarke[10], N. De Luca[26], F. Dentener[16], T. Diehl[17], O. Dubovik[14], R. Easter[18], D. W. Fahey[9], J. Feichter[4], D. Fillmore[23], S. Freitag[10], S. Ghan[18], P. Ginoux[19], S. Gong[20], L. Horowitz[19], T. Iversen[13,28], A. Kirkevåg[28], Z. Klimont[7], Y. Kondo[11], M. Krol[12], X. Liu[25,18], C. McNaughton[10], R. Miller[2], V. Montanaro[25], N. Moteki[11], G. Myhre[13,21], J. E. Penner[24], Ja. Perlwitz[1,2], G. Pitari[25], S. Reddy[14], L. Sahu[11], H. Sakamoto[11], G. Schuster[5], J. P. Schwarz[9], Ø. Seland[28], J. R. Spackman[9], P. Stier[26], N. Takegawa[11], T. Takemura[27], C. Textor[3], J. A. van Aardenne[8], and Y. Zhao[22]

[1]Columbia University, New York, NY, USA
[2]NASA GISS, New York, NY, USA

[3] Laboratoire des Sciences du Climat et de l'Environnement, Gif-sur-Yvette, France
[4] Max-Planck-Institut fur Meteorologie, Hamburg, Germany
[5] NASA Langley Research Center, Hampton, Virginia, USA
[6] University of Illinois at Urbana-Champaign, Urbana, IL, USA
[7] International Institute for Applied Systems Analysis, Laxenburg, Austria
[8] European Commission, Institute for Environment and Sustainability, Joint Research Centre, Ispra, Italy
[9] NOAA Earth System Research Laboratory, Chemical Sciences Division and Cooperative Inst. for Research in Environmental Sciences, University of Colorado, Boulder, Colorado, USA
[10] University of Hawaii at Manoa, Honolulu, Hawaii, USA
[11] RCAST, University of Tokyo, Japan
[12] Meteorology and Air Quality, Wageningen University, Wageningen, The Netherlands
[13] University of Oslo, Oslo, Norway
[14] Universite des Sciences et Technologies de Lille, CNRS, Villeneuve d'Ascq, France
[15] NASA Goddard Space Flight Center, Greenbelt, MD, USA
[16] EC, Joint Research Centre, Institute for Environment and Sustainability, Italy
[17] University of Maryland Baltimore County, Baltimore, Maryland, USA
[18] Battelle Pacific Northwest Division, Pacific Northwest National Laboratory, Richland, USA
[19] NOAA, Geophysical Fluid Dynamics Laboratory, Princeton, New Jersey, USA
[20] ARQM Meteorological Service Canada, Toronto, Canada
[21] Center for International Climate and Environmental Research – Oslo (CICERO) Oslo, Norway
[22] University of California – Davis, CA, USA
[23] NCAR, Boulder, CO, USA
[24] University of Michigan, Ann Arbor, MI, USA
[25] Universita degli Studi L'Aquila, Italy
[26] Atmospheric, Oceanic and Planetary Physics, University of Oxford, UK

ACPD
9, 15769–15825, 2009

[27] Kyushu University, Fukuoka, Japan
[28] Norwegian Meteorological Institute, Oslo, Norway

Received: 1 July 2009 – Accepted: 18 July 2009 – Published: 24 July 2009

Correspondence to: D. Koch (dkoch@giss.nasa.gov)

Published by Copernicus Publications on behalf of the European Geosciences Union.

Abstract

We evaluate black carbon (BC) model predictions from the AeroCom model intercomparison project by considering the diversity among year 2000 model simulations and comparing model predictions with available measurements. These model-measurement intercomparisons include BC surface and aircraft concentrations, aerosol absorption optical depth (AAOD) from AERONET and Ozone Monitoring Instrument (OMI) retrievals and BC column estimations based on AERONET. In regions other than Asia, most models are biased high compared to surface concentration measurements. However compared with (column) AAOD or BC burden retreivals, the models are generally biased low. The average ratio of model to retrieved AAOD is less than 0.7 in South American and 0.6 in African biomass burning regions; both of these regions lack surface concentration measurements. In Asia the average model to observed ratio is 0.6 for AAOD and 0.5 for BC surface concentrations. Compared with aircraft measurements over the Americas at latitudes between 0 and 50 N, the average model is a factor of 10 larger than observed, and most models exceed the measured BC standard deviation in the mid to upper troposphere. At higher latitudes the average model to aircraft BC is 0.6 and underestimates the observed BC loading in the lower and middle troposphere associated with springtime Arctic haze. Low model bias for AAOD but overestimation of surface and upper atmospheric BC concentrations at lower latitudes suggests that most models are underestimating BC absorption and should improve estimates for refractive index, particle size, and optical effects of BC coating. Retrieval uncertainties and/or differences with model diagnostic treatment may also contribute to the model-measurement disparity. Largest AeroCom model diversity occurred in northern Eurasia and the remote Arctic, regions influenced by anthropogenic sources. Changing emissions, aging, removal, or optical properties within a single model generated a smaller change in model predictions than the range represented by the full set of AeroCom models. Upper tropospheric concentrations of BC mass from the aircraft measurements are suggested to provide a unique new benchmark to test scavenging

ACPD

9, 15769–15825, 2009

and vertical dispersion of BC in global models.

1 Introduction

Black carbon, the strongly light-absorbing portion of carbonaceous aerosols, is thought to contribute to global warming since pre-industrial times. It is a product of incomplete combustion of both fossil fuels and biofuels, such as coal, wood and diesel. Black carbon (BC) has several effects on climate, primarily warming, but potentially also some amount of cooling. The "direct effect" is the scattering and absorption of incoming solar radiation by the BC suspended in the atmosphere. The absorption warms the air where the BC aerosol is suspended, but the extinction of radiation results in negative forcing at the earth's surface. The "BC-albedo effect" occurs because black carbon deposited on snow lowers the snow albedo and may therefore promote snow and ice melting. BC may also have important effects on clouds by changing atmospheric stability and/or relative humidity, and thus affect cloud formation; this has been termed the "semi-direct effect". Finally, BC is a primary aerosol particle and influences the number of particles available for cloud condensation; it may thus play an important role for the aerosol cloud "indirect effect". BC may also affect the indirect effect by acting as ice nuclei.

Quantifying the effects of black carbon on climate change is hindered by several uncertainties. Emissions are uncertain because of difficulties quantifying sources and emission factors (e.g. Bond et al., 2004). Measurements of BC concentrations are uncertain because of instrumental limitations in the present measurement techniques (Andreae and Gelencser, 2006). Optical properties are uncertain since these vary with source, morphology, particle age and chemical processing. Atmospheric column aerosol absorption comes mostly from black carbon in many polluted and biomass burning regions. This absorption aerosol optical depth (AAOD) has been retrieved from satellite and an array of sunphotometer measurements, and these retrievals also help to constrain column BC. However the constraint is limited by uncertainties and assump-

ACPD
9, 15769–15825, 2009

tions in the retrievals as well as by the fact that other absorbing species besides BC are present, such as dust and organic carbon. Model simulation of BC is complicated by uncertainties in treatment of initial particle size and shape appropriate for initial release in a model gridbox, particle uptake in liquid or frozen clouds and precipitation, treatment of mixing state and optical properties. Assumptions influencing the degree of internal vs. external mixing with water-soluble particles in the accumulation mode strongly influence the aerosol absorption (Seland et al., 2008) and CCN-activation. Internal mixing of BC also affects BC lifetime, decreasing it relative to insoluble BC (Stier et al., 2006, 2007). Furthermore, the BC model predictions are subject to model uncertainties that apply to any chemical model simulation, such as the accuracy of the model's meteorology (transport, clouds, precipitation).

The aim of this study is to evaluate model-calculated BC in recent state-of-the-art global models with aerosol chemistry and physics, to consider their diversity and compare them with available observations. There has been concern that some models may greatly underestimate BC absorption and therefore BC contribution to climate warming (e.g. Sato et al., 2003; Ramanathan and Carmichael, 2008; Seland et al., 2008). However it is unclear whether this is a problem common to all models, whether the problem is regional or global, and the extent to which the bias is due to BC mass underestimation possibly linked to emissions underestimation, or to model treatment of optical properties leading to underestimation of BC absorption. We examine these issues by comparing the models to a variety of measurements, and working with a large number of current models. We also investigate whether biases in some regions are more problematic than in others. Finally we make use of one of the models, the GISS model (available to the first author of this paper), to consider the effects of changing BC emissions, aging, removal assumptions and optical properties. We also use the GISS model to consider the seasonality of model bias and the spectral dependence of AAOD bias.

We compare the models with several types of observations. Model surface concentrations are compared with long-term surface concentration measurements. Model BC

ACPD
9, 15769–15825, 2009

concentration profiles are compared with aircraft measurements for several recent aircraft campaigns, spanning the North American region from the tropics to the Arctic. Column BC is assessed by comparing model aerosol absorption optical depth (AAOD) with AAOD retrieved by Dubovik and Kings' (2000) inversion algorithm from AERONET sunphotometer measurements (Holben et al., 1998), as was done in Sato et al. (2003), and with OMI satellite retrievals of AAOD. We also compare column burden of BC with the AERONET-based estimation as in Schuster et al. (2005). While the measurements provide constraints for the models, in the final section we will discuss measurement uncertainties and the discrepancies among them that are apparent as we apply them to the models.

2 Model descriptions

2.1 AeroCom models

We evaluate seventeen models from the AeroCom aerosol model intercomparison, an exercise that has been ongoing for the past 5 years. Model results, as well as observation datasets for validation purposes, are available at the AeroCom website (http://nansen.ipsl.jussieu.fr/AEROCOM/). The AeroCom intercomparison exercises included an exercise "A" with each model using its own emissions, and an exercise "B" where all models used identical emissions, and are described in detail in Textor et al. (2006, 2007), Kinne et al. (2006) and Schulz et al. (2006). Here we work with exercise A unless only B is available for a particular model in the database. The models used year 2000 emissions and in some cases year 2000 meteorological fields. Not all diagnostics were available for all models, so we used all those available for each quantity considered. Many aspects of the models have been evaluated in previous publications, and we refer to those for general background information. Textor et al. (2006) provides a first comparison of the models in experiment A and includes basic information on the models such as model resolution, chemistry, removal assumptions.

ACPD
9, 15769–15825, 2009

Textor et al. (2007) describes the exercise B model intercomparison, and showed that model diversity was not greatly reduced by unifying emissions, indicating that the greatest model differences result from features such as meteorology and aerosol treatments rather than from emissions. Kinne et al. (2006) discusses the aerosol optical properties of the models and Schulz et al. (2006) presents the radiative forcing estimates for the models.

Some of the model features most relevant for the BC simulations are provided in Table 1. As shown there, five different BC energy emissions inventories and eleven different biomass burning emissions inventories were used. The models had a variety of schemes to determine black carbon aging from a fresh to aged particle, where aged particles are activated into cloud water. Nine models assumed that black carbon aged from insoluble to soluble after a fixed lifetime; five models had microphysical mixing schemes to make the particles soluble, in one model the black and organic carbon are assumed to be mixed when emitted, and one model had fixed solubility. In two cases the particle mixing affected optical/radiative properties. A variety of assumptions were made about how frozen clouds removed aerosols compared to liquid clouds, ranging from identical treatments for frozen and liquid clouds to zero removal by ice clouds. Black carbon lifetime ranges from 4.9 to 11.4 days.

We note that the model versions evaluated here were submitted to the database in year 2005, and some of the models have evolved significantly since (e.g. Stier et al., 2006, 2007; Ghan and Zaveri, 2007; Bauer et al., 2008). Thus this study provides a benchmark at the time of the 2005 submission.

2.2 GISS model sensitivity studies

We use the GISS aerosol model to study sensitivity to some factors that could impact the BC simulation. The GISS aerosol scheme used here includes mass of sulfate, sea-salt (Koch et al., 2006), carbonaceous aerosols (Koch et al., 2007) and dust (Miller et al., 2006; Cakmur et al., 2006). The sensitivity studies are described below and are listed in Table 2. All simulations are performed and averaged for 3 years, after a 2-year

model spin-up. The standard GISS model version for these sensitivity studies is slightly different than the version in the AeroCom database. This version does not include dust-nitrate interaction, and does not include enhanced removal of BC by precipitating convective clouds as was included in the AeroCom-database GISS model version, and therefore has a somewhat larger BC load.

2.2.1 Emissions

The standard model uses carbonaceous aerosol energy production emissions from Bond et al. (2004). Biomass burning emissions are based on the Global Fire Emissions Database (GFED) v2 model carbon estimates for the years 1997–2006 (van der Werf et al., 2003, 2004), with the carbonaceous aerosol emission factors from Andreae and Merlet (2001). One sensitivity case had fossil and biofuel emissions from EDGAR4 combined with emissions factors from Bond et al. (2004) (preliminary EDGAR4 dataset provided by J. van Aardenne) and in another those of IIASA (Cofala et al., 2007). In a third we used the largest biomass burning year from the GFED dataset, 1998.

2.2.2 Aging and removal

In the standard model, energy-related BC is assumed to have no cloud-water uptake initially and then ages to become soluble with an e-fold lifetime of 1 day. Biomass burning BC is assumed to have 60% solubility, so that if a cloud is present, 60% these aerosols are taken into the cloud water for each half-hour cloud timestep. One sensitivity test assigned a shorter lifetime with a halved e-folding time for energy BC and 80% solubility for biomass burning. A second case assumes a longer lifetime, with doubled e-folding time for energy BC and 40% solubility for biomass burning.

Treatment of BC solubility is particularly uncertain for frozen clouds. In our standard model, BC-cloud uptake for frozen clouds is 12% of that for liquid clouds. A sensitivity run allowed 24% ice-cloud BC uptake, and another case 5%.

2.2.3 Aerosol size

The standard model assumes the BC effective radius (cross section weighted radius over the size distribution, Hansen and Travis, 1974) is 0.08 μm. One sensitivity case increased this to 0.1 μm, and another decreased it to 0.06 μm. The size primarily affects the BC optical properties. For BC sizes 0.1, 0.08 and 0.06 μm, the model global mean BC mass absorption efficiencies are 6.2, 8.4 and 12.4 and BC single scattering albedos are 0.31, 0.27 and 0.21.

3 Model evaluation

3.1 Surface concentrations

Annual average BC surface concentration measurements are shown in the first panel of Fig. 1. The data for the United States are from the IMPROVE network (1995–2001) and those from Europe are from the EMEP network (2002–2003); some Asian data from 2006 are from Zhang et al. (2009); additional data, mostly from the late 1990s, are referenced in Koch et al. (2007). These data are primarily elemental carbon, or refractory carbon, which can be somewhat larger than BC. There are general regional differences, with largest concentrations in Asia (1000–14 000 ng m^{-3}), then Europe (500–5000 ng m^{-3}), then the United States (100–500 ng m^{-3}), then high northern latitudes (10–100 ng m^{-3}) and least at remote locations (<10 ng m^{-3}).

Figure 1 also shows BC surface concentrations from the GISS model sensitivity studies. The biggest impact for remote regions comes from increasing BC lifetime, either by doubling the aging rate or by reducing the removal by ice. Decreasing the BC lifetime has a smaller effect. The larger 1998 biomass burning emissions mostly increases BC in boreal Northern Hemisphere and Mexico. EDGAR emissions increase BC in Europe, Arabia and northeastern Africa; IIASA emissions increase South Asian BC.

Figure 2 shows the AeroCom model simulations of BC surface concentration, along

ACPD
9, 15769–15825, 2009

with the average and standard deviations of the models. The standard deviation distribution is similar to the average. Regions of especially large model uncertainty occur where the standard deviation equals or exceeds the average, such as the Arctic. Overall the models capture the observed distribution of BC "hot spots". Only the SPRINTARS model successfully captures the large BC concentrations in Southeast Asia, however that model overestimates BC in other regions. Unfortunately there are no long-term measurements of BC in the Southern Hemisphere biomass burning regions.

Table 3 shows the ratio of modeled to observed BC in regions where surface concentration observations are available. The regional ratios are based on the ratio of annual mean model to annual mean observed for each site, averaged over each region. Eleven out of thirteen AeroCom models over-predict BC in Europe. Twelve of the models underestimate Southeast Asian BC surface concentrations; however most of these measurements are from 2004–2006 and emissions have probably increased significantly since the 1990s (Zhang et al., 2009). Nine out of the 14 models overestimate remote BC; in the United States about half the models overestimate and half underestimate the observations. Overall, the models do not underestimate BC relative to the in situ measurements. None of the GISS model sensitivity studies show significant improvement over the standard case. The longer lifetime cases improve the model-measurement agreement in polluted regions but worsen the agreement in remote regions.

3.2 Aerosol absorption optical depth

The aerosol absorption optical depth (AAOD), or the non-scattering part of the aerosol optical depth, provides another test of model BC. AAOD is an atmospheric column measure of particle absorption, and so provides a different perspective from the surface concentration measurements. Both BC and dust absorb radiation, so AAOD is most useful for testing BC in regions where it dominates over dust absorption. Therefore we focus on regions where the dust load is relatively less, for example Africa south of the

Sahara Desert. However since some sites within these regions still have significant dust, we work with model AAOD for all species.

Figure 3 shows AERONET (1996–2006) sunphotometer and OMI satellite (2005–2007, from OMAERUV product) retrievals of clear sky AAOD. A scatter plot compares the AERONET and OMI retrievals at the AERONET sites. Table 4 (last 5 rows) provides regional average AAOD for these retrievals. The two retrievals broadly agree with one another. However, the OMI estimate is larger than the AERONET value for South America and smaller for Europe and Southeast Asia.

The AeroCom model AAOD simulations are in Fig. 4. The standard deviation relative to the average is similar to the surface concentration result; it is less than or equal to the average, except in parts of the Arctic. Table 4 gives the average ratio of model to retrieved AAOD within regions. For the ratio of model to AERONET we average the model AAOD over all AERONET sites within the region and divide by the average of the corresponding AERONET values. For OMI we average over each region in the model and divide by the OMI regional average. The average model agrees with the retrievals in eastern North America and with AERONET in Europe (ratios of modeled to AERONET in these regions are 0.82 and 0.75); it underestimates Asian (ratio is 0.6) and biomass burning AAOD (about 0.6 for AERONET and 0.4 for OMI).

AAOD depends not just on aerosol load but also on optical properties, such as refractive index, particle size, density and mixing state. In Fig. 3 we show how the GISS model AAOD changes with assumed effective radius. The global mean AAOD decreases/increases 15%/27% for an increase/decrease of 0.02 μm effective radius. Note that the AeroCom model initial particle diameters (Table 1) span beyond this range (0.02 to 0.9 μm) and in some cases grow as the particles age. Increasing particle density from 1.6 to 1.8 g cm^{-3} in the GISS model decreases AAOD about as much as increasing particle size from 0.08 to 0.1 μm (calculated but not shown). Thus the AAOD is highly sensitive to small changes in these optical properties.

Note that models generally underestimate AAOD but not surface concentration. As we will discuss below, this could result from inconsistencies in the measurements or

ACPD
9, 15769–15825, 2009

from model under-prediction of BC aloft or under-prediction of absorption. In this connection most models in the 2005-version of AeroCom did not properly describe internal mixing with scattering components in the accumulation mode. Such mixing increases the absorption cross section of the aerosols compared to external mixtures of nucleation- and Aitken-mode BC particles.

3.3 Wavelength-dependence

Black carbon absorption efficiency decreases less with increasing wavelength compared with dust or organic carbon (Bergstrom et al., 2007). Therefore comparison of AAOD with retrievals at longer wavelength indicates the extent to which BC is responsible for biases. In Fig. 5 we compare AERONET AAOD at 550 and 1000 nm with the GISS model AAOD for the wavelength intervals 300–770 nm and 860–1250 nm, respectively. Table 5 shows the ratio of the GISS model to AERONET within source regions for 1000 nm and 550 nm, for three different BC effective radii. In all regions except Europe and Asia, the ratio is even lower at the longer wavelength, confirming the need for increased simulated BC absorption, rather than other absorbing aerosols that absorb relatively less at longer wavelengths.

3.4 Seasonality

Our analysis has considered only annual mean observed and modeled BC. Here we present the seasonality of observed AAOD compared with the GISS model to explore how the bias may vary with season. Seasonal AAOD are shown for AERONET, OMI and the GISS model in Fig. 6. As in most of the models, the GISS model BC energy emissions do not include seasonal variation. Biomass burning does, and dust seasonality is also very pronounced. However, transport and removal seasonal changes also cause fluctuations in model industrial source regions. Note that more AERONET data satisfy our inclusion criteria for the 3 month means compared with annual means (given in the figure captions), so coverage is better in some regions and seasons than

ACPD
9, 15769–15825, 2009

in the annual dataset in Fig. 3. Table 4 (bottom 4 rows) gives regional seasonal retrieved mean AAOD. The seasonal model-to-measurement ratios are also provided in the middle portion of Table 4.

Biomass burning seasonality, with peaks in JJA for central Africa (OMI) and in SON for South America, is simulated in the model without clear change in bias with season. In Asia both retrievals have maximum AAOD in MAM, which the model underestimates (i.e. ratio of model to observed is lowest in MAM). The MAM peak may be from agricultural or biomass burning not captured by the model. The other industrial regions do not have apparent seasonality. However the model BC is underestimated most in Europe during fall and winter suggesting excessive loss of BC or missing emissions during those seasons.

Summertime pollution outflow from North America seems to occur in both OMI and the model. The large OMI AAOD in the southern South Atlantic during MAM-JJA may be a retrieval artifact due to low sun-elevation angle and/or sparse sampling; however if it is real, then the seasonality in the model in this region is out of phase.

3.5 Column BC load

Model simulation of column BC mass (Fig. 7) in the atmosphere should be less diverse than the AAOD since it contains no assumptions about optical properties. However there is no direct measurement of BC load. Schuster et al. (2005) developed an algorithm to derive column BC mass from AERONET data, working with the non-dust AERONET climatologies defined by Dubovick et al. (2002). The Schuster algorithm uses the Maxwell Garnett effective medium approximation to infer BC concentration, and specific absorption from the AERONET refractive index. The Maxwell Garnett approximation assumes homogeneous mixtures of small insoluble particles (BC) suspended in a solution of scattering material. Such mixing enhances the absorptivity of the BC. Schuster et al. (2005) estimated an average specific absorption of about $10\,m^2\,g^{-1}$, a value larger than most of the models (see Table 1).

An updated version of the AERONET-derived BC column mass is shown in the lower

ACPD
9, 15769–15825, 2009

right panels of Figs. 7 and 8. For this retrieval, a BC refractive index of 1.95–0.79i was assumed, within the range recommended by Bond and Bergstrom (2006), and BC density of 1.8 g cm^{-3}. In the retrievals, most continental regions have BC loadings between 1 and 5 mg m^{-2}, with mean values for North America (1.8 mg m^{-2}) and Europe (2.1 mg m^{-2}) being somewhat smaller than Asia (3.0 mg m^{-2}) and South America (2.7 mg m^{-2}). The current industrial region retrievals are larger than the previous estimates of Schuster et al. (2005), which were 0.96 mg m^{-2} for North America, 1.4 mg m^{-2} for Europe and 1.6 mg m^{-2} for Asia. The biomass burning estimates are similar to the previous retrievals. The differences may be due to the larger span of years and sites in the current dataset.

Figure 7 shows the AeroCom model BC column loads. The model standard deviation relative to the average is similar to the surface concentration (Fig. 2) and the AAOD (Fig. 4). The model column loads are smaller than the Schuster estimate, especially in North and South America. Some models agree quite well in Europe, Southeast Asia or Africa (e.g. GOCART, SPRINTARS, MOZGN, LSCE, UMI). Model to retrieved ratios within selected regions are presented in Table 6. This ratio is generally smaller than model to retrieved AAOD in North America and Europe. The inconsistencies among the retrievals would benefit from detailed comparison with a model that includes particle mixing and with model diagnostic treatment harmonized to the retrievals.

Figure 8 has GISS BC column sensitivity study results. The load is affected differently than the surface concentrations (Fig. 1). The Asian IIASA emissions are larger than Bond or EDGAR, so that the outflow across the Pacific is greater. The large-biomass burning case (1998) also results in greater BC transport to Northwestern US in the column. Increasing BC lifetime increases both BC surface and column mass more than the other cases; however it has a larger impact on Southern Hemisphere load than surface concentrations. The reduced ice-out case has somewhat smaller impact on the column than at the surface, especially for some parts of the Arctic.

ACPD
9, 15769–15825, 2009

3.6 Aircraft campaigns

We consider the BC model profiles in the vicinity of recent aircraft measurements in order to get a qualitative sense of how models perform in the mid-upper troposphere and to see how the model diversity changes aloft. The measurements were made with three independent Single Particle Soot absorption Photometers (SP2s) (Schwarz et al., 2006; Slowik et al., 2007) onboard NASA and NOAA research aircraft at tropical and middle latitudes (Fig. 9) and at high latitudes (Fig. 10) over North America. Details for the campaigns are provided in Table 7. The SP2 instrument uses an intense laser to heat the refractory component of individual aerosols in the fine (or accumulation) mode to vaporization. The detected thermal radiation is used to determine the black carbon mass of each particle (Schwarz et al., 2006). The BC mass observed is extrapolated to represent the total BC mass associated with the fine mode for the NOAA in situ data presented in Fig. 9a, b, c and Fig. 10c. For these data, the actual measured fraction (not shown) varied from 60 to 90%. In contrast, only the measured BC mass is plotted in Fig. 9d, e and Fig. 10a, b, d, e and results in an underestimation of the total BC mass in the fine mode by 10 to 20%. Note that smaller or larger modes of BC are not measured and are not expected in aged airmasses. The University of Tokyo spring data are split between the midlatitudes (Fig. 9d) and Arctic (Fig. 10a). The aircraft data in each panel of Figs. 9 and 10 are averaged into altitude bins along with standard deviations of the data. For cases where the aircraft encountered significant biomass burning smoke, the data are either separated into smoky and remote profiles (Fig. 10c, dashed and solid, respectively) or the median is also provided as more indicative of background conditions (dashed, Fig. 10d, e). Model profiles shown in each panel are constructed by averaging monthly mean model results at several locations along the flight tracks (map symbols in Figs. 9 and 10). We tested the accuracy of the model profile-construction approach using the University of Tokyo data and the GISS model, by comparing a profile constructed from following the flight tracks within the model fields with the simpler profile construction shown in Figs. 9–10. The

ACPD
9, 15769–15825, 2009

two approaches agreed very well except in the boundary layer (the lowest 1–2 model levels). Potentially more problematic is the comparison of instantaneous observational snapshots to model monthly means. Nevertheless the comparison does suggest some broad tendencies.

The lower-latitude campaign observations (Fig. 9), with the exception of the midlatitude University of Tokyo data that represent samples over the ocean (Fig. 9d), indicate polluted boundary layers with BC concentrations decreasing 1–2 orders of magnitude between the surface and the mid-upper troposphere. Some of the large data values can be explained by sampling of especially polluted conditions. For example, the CARB campaign (Fig. 9e) encountered unusually heavy biomass burning, and the University of Tokyo data over the Pacific (Fig. 9d) included sampling of a pollution plume during one of the flights. The models would not have included these particular fire conditions. Nevertheless, the datasets show remarkably consistent mid-tropospheric mean BC levels of about 0.5–5 ng/kg in the tropics and midlatitudes. Most models are within the data standard deviations up to about 700 mb (Fig. 9c, d, e), while exceeding the upper limit of the observed standard deviation above 500 mb (Fig. 9b, c, e).

The spring-time Arctic campaigns observed maximum BC above the surface (Fig. 10a, b, c), which may occur from two mechanisms. First, background "Arctic haze" pollution is thought to originate at lower latitudes, and is transported to the Arctic by meridionally lofting along isentropic surfaces (Iversen, 1984; Stohl et al., 2006). Most of the observed profiles and the model results would reflect those conditions. Alternatively, BC could be injected into the mid-troposphere near its source by agricultural or forest fires and then advected into the Arctic. This is apparently the case for the ARCPAC measurements (dashed black line in Fig. 10c) that probed Russian fire smoke (Warneke et al., 2009). In both cases, the pollution levels aloft during springtime are substantial and comparable to those levels observed in the polluted boundary layer at midlatitudes. Model profile diversity is especially great in the Arctic, as discussed in previous sections. Many of the models do have profile maximum BC above the surface, but most of the springtime peak values are smaller in magnitude than the

ACPD
9, 15769–15825, 2009

aircraft measurements. The three spring campaign measurements have mean BC of about 50–100 ng kg^{-1} at 500 mb; 9 of the models are less than 20 ng kg^{-1} while 6 of them are within the observed range. This means that most models are underestimating poleward transport, are removing the BC too efficiently or are not confining pollution sufficiently to the lowest model levels due to excessive vertical diffusion.

The high-latitude summer ARCTAS campaigns encountered heavy smoke plumes for part of their campaign, so the mean (Fig. 10d–e, solid black) values are less characteristic of typical conditions than the median (dashed). The models include climatological biomass burning emissions. Most models are within the observed standard deviation for the summertime data however overestimate BC above 500 mb. The models seem to have little change in estimates between spring and summer (compare Fig. 10b and d), while the observed background conditions are less polluted in summer. Similar to the lower latitudes, the models generally overestimate BC in the lower stratosphere (Fig. 10a) and upper troposphere (Fig. 10d, e) in the Arctic. On the other hand, the upper troposphere-lower stratosphere measurements in the Arctic region are sparse and may not be statistically significant.

The ratio of model to observed BC over the profiles for Fig. 9a–c (south) and Fig. 10 (north), excluding the bottom 2 layers of each model, are given in Table 8. The average model ratio is 10.4 in the south and 0.56 in the north. In general, the ordering of model concentrations in the mid-troposphere is the same across latitudes, so the models with small upper tropospheric concentrations in the tropics also are smaller in the Arctic. Typically those that are most successful compared to the observations at low latitudes do not have large enough concentrations in the lower and middle troposphere in the Arctic. This could result from failure to distinguish between removal of BC by convective and stratiform clouds, with convective clouds providing deep-column cleaning of particles primarily at lower latitudes. The models may also fail to resolve pollution transport events needed to bring pollution to the Arctic. However, some models are fairly versatile; for example the MIRAGE, UMI and GISS models attain large lower tropospheric concentrations in the Arctic yet relatively low concentrations aloft at low latitudes; these

ACPD
9, 15769–15825, 2009

are within a factor of 5 of observed in the south and a factor of 2 in the north (Table 8). Some of the models have a strong minimum at around 300–400 hPa, probably due to effective scavenging in a region where condensable water tends to be removed by rain. This seems to work well in the lower latitude regions, however it apparently should not apply at the higher latitudes where colder clouds dominate.

We also made profiles for the GISS sensitivity simulations. However the variability among these cases is much smaller than for the AeroCom models in Figs. 9–10. Doubling or halving the GISS BC aging rate generally made the lowest and highest concentrations, respectively, throughout the column, however the difference was less than a factor of two from the standard case. In the Arctic near the surface the case with increased ice-out had the lowest concentration, but again the change was not large.

3.7 Summary of model-observation comparison

The average AeroCom model performance compared to each measurement type for each region is given in Table 9. The average model bias tends to be high compared with surface concentration measurements, in all regions except Asia. The average model bias tends to be low compared with all column retrievals in regions other than the OMI estimate for Europe. The model bias is especially low in biomass burning regions of Africa and South America; unfortunately there are no long-term surface concentration measurements in these regions to help discriminate errors in biomass burning emissions from optical properties. It is also likely that anthropogenic emissions are underestimated, especially in South America (e.g. Evangelista et al., 2007). The rest-of-world bias is quite low for the column quantities; however the retrievals tend to have greater difficulty for small aerosol optical depth conditions (e.g. Dubovik et al., 2002) and may therefore be biased high. A detailed analysis in which the model diagnostics are screened with the same criteria as AERONET would help to resolve this. The remote BC load is sensitive to the BC aging or mixing rate, so resolving the discrepancy is important. It is possible that model aging rate is overestimated in the models, resulting in excessive removal and low model bias away from source regions.

ACPD
9, 15769–15825, 2009

North America is the only region where we have SP2 aircraft measurements, and generally the models are larger than observed both at the surface and in the free troposphere. The models underpredict AAOD and the Schuster-BC in North America, but the comparison with aircraft data suggests that the models are actually overestimating middle-upper atmospheric BC. It therefore seems that the optical properties in the models provide less absorption than they should, or that the retrievals overestimate AAOD, or that the treatment of the model diagnostic is not sufficiently harmonized to the retrieval.

4 Discussion and conclusions

Our comparison of AeroCom models and observations reveals some large BC discrepancies and diversities. To some extent the comparison of AeroCom and GISS sensitivity models can be used to infer which parameters might improve performance.

The AeroCom models use a variety of BC emission inventories (Table 1). In the GISS sensitivity studies we used three recent inventories and did not see dramatic differences in the model results, however the developers of these inventories shared similar energy and emission factor information so it is not surprising that the inventories are not very different, although for specific regions there are some large differences. Furthermore, this is consistent with the Textor et al. (2007) comparison of model experiments with and without different emissions in which model diversity was not greatly reduced if the emissions were harmonized. It therefore seems that the lowest order model biases require either changes to BC in most inventories, or changes to other model characteristics.

The BC inventories continue to improve as information on technologies and activities become available, especially in developing countries. In addition, it seems likely that model results could derive as much benefit from the addition of optical property information specific for individual emission sources, such as particle size, density and mixing state appropriate for model grid-box-scale sources. Biomass burning emission

ACPD
9, 15769–15825, 2009

estimations are also improving. For example, the latest GFED estimates rely on satellite observations of burned area and fire counts in deriving the burning history (Giglio et al., 2006; van der Werf et al., 2006). Here we only considered seasonal variability in the GISS model, and it seemed to agree reasonably well compared with retrieved AAOD seasonality in the biomass burning regions. On the other hand, nearly all models underestimate column BC in these regions, especially in South America, suggesting that the emission factors (currently based on Andreae and Merlet, 2001) or optical properties for the smoke are not generating enough BC and/or particle absorption. Spackman et al. (2008) reported BC emission factors from fresh biomass burning plumes that were 25 to 75% higher than those reported in Andreae and Merlet (2001), consistent with the model underestimations noted here. Long-term in situ measurements co-located with AERONET sites could help resolve which of these is in error.

Many models are developing sophisticated aerosol microphysical processes, including information on nucleation, evolving particle size distributions, particle coagulation and mixing by condensation of gases onto particles. The added physical treatment also allows more physical representation of particle solubility, optical properties, uptake into clouds, etc. However it is challenging to increase physical sophistication in the schemes while validating the schemes using field information on how such particles behave in the real world. The assessment here includes some constraint on final BC properties. While microphysical schemes are essential for simulating particle number and size distribution, it is not apparent that they improve on BC simulation as examined here. Yet the schemes might benefit from increased sophistication, such as including evolution of particle morphology, effect of internal mixing on particle absorption, and density (Stier et al., 2007).

Indeed, Bond and Bergstrom (2006) have provided some straightforward recommended improvements for BC models, but many models presented here had not yet included these. Bond and Bergstrom suggested a typical fresh particle mass absorption cross section (MABS, essentially the column BC absorption divided by the load) of about $7.5\,m^2\,g^{-1}$ and that this should probably increase as particles age. Nine of

ACPD
9, 15769–15825, 2009

the models have MABS larger than 6.7 $m^2\,g^{-1}$. Enhancement of absorption from BC coating was recommended to be about a factor of 1.5 and this has not been included in the models. A recent study with the UIOCTM did include a 1.5 enhancement of MABS for aged BC and found increased radiative forcing of 28% (Myhre et al., 2009). Bond and Bergstrom recommended refractive index values larger than the value used in older models, i.e. about 1.9–0.7i at 550 nm; three of the models have values larger than 1.9–0.6i. Bond and Bergstrom also pointed out that many models have underestimated particle density and recommend a value of about 1.7–1.9 $g\,cm^{-3}$. Five of the models have densities lower than this range and would have weaker absorption if the density was increased to the recommended level. In summary, including particle core-shell configuration, and increasing refractive index should increase model particle absorption, while increasing density will decrease AAOD.

Model treatment of BC solubility and uptake by clouds is determined by assuming a fixed uptake rate or solubility, or by assuming the BC becomes soluble following some aging time, or from a microphysical scheme that includes mixing with soluble species. Relatively little effort has been given to treatment of BC uptake by frozen clouds. Some field information is available, e.g. Cozic et al. (2007), and although more observations are needed, this is a process models need to consider more carefully. The comparison of models with aircraft data (Figs. 9–10) suggests that some upper-level removal processes may be missing. Alternatively the model vertical mixing may be excessive. It would be useful for the models to compare other species with available aircraft observations to learn whether the bias is primarily for BC or occurs also for other species. The GISS model is fairly successful at capturing the decrease with altitude for SO_2, sulfate, DMS and H_2O_2 (Koch et al., 2006). We have had some success decreasing the BC aloft in the GISS model by enhancing removal by convective clouds. The ECHAM5 model has found improved vertical transport results with increased vertical resolution. Note however, that decreasing the load of BC diminishes the AAOD and worsens that bias.

An obvious difficulty in applying the various datasets for model constraint is the un-

ACPD
9, 15769–15825, 2009

certainty in the data. Thorough discussion of this topic is beyond the scope of this study but we briefly summarize some issues here. There are uncertainties in surface measurements and AAOD retrievals, failure to accurately account for additional absorbing species, differing treatments of model diagnostics and retrievals, and mismatch of periods for observations and model.

Surface concentration measurements are made by a variety of techniques, including various thermal and optical approaches, summarized in e.g. Bond and Bergstrom (2006). This variety contributes to bias scatter in the model evaluations. In particular, the reflectance method used for IMPROVE is known to measure higher EC than the transmittance method used by EMEP (Chow et al., 2001), which may explain some of the difference in model-measurement comparisons between different regions.

AERONET and OMI retrievals of AAOD use uniform techniques for their respective retrievals, however they have their own uncertainties. The AERONET retrieval algorithm (Dubovik and King, 2000) derives detailed size distribution and spectrally dependent complex refractive index by fitting direct and transmitted diffuse radiation measured by ground-based sun-photometers (Holben et al., 1998). No microphysical model is assumed for size distribution or for complex refractive index. Then the values of AAOD are calculated using the combination of size distribution and index of refraction that provide best fit to the measurements. The major limitation for the retrieval of aerosol absorption is caused by the limited accuracy of the direct Sun radiation measurements (Dubovik et al., 2000). As shown by Dubovik et al. (2000), the retrieval of aerosol absorption and Single Scattering Albedo (SSA=scattering/(scattering+absorption)), are unreliable at low aerosol loading conditions, with AAOD tending to be biased high but with accuracy of 0.01.

Although no similar limitation has been documented for the OMI retrieval, generally the accuracy of OMI retrievals (as for the retrievals by any other passive satellite sensors) is also lower for lower aerosol loading conditions since the aerosol signal to radiometric noise ratio decreases. The OMI retrieval also relies on a predetermined

ACPD
9, 15769–15825, 2009

limited set of aerosol models and the OMI algorithm chooses the model as part of the retrieval. Then the AAOD as well as other aerosol parameters (including Angstrom parameter) are estimated using the retrieved aerosol optical depth (AOD) and chosen model. Obviously, the incorrect choice of the aerosol model would affect the retrievals of both AAOD and angstrom parameter. In contrast, the AERONET retrieval uses transmitted radiation (not reflected as registered by OMI) and the angstrom parameter is derived from direct AOD measurements (not an aerosol model).

Both AERONET and OMI data are also for daytime and clear-sky conditions only, and the model results used here are all-day and all-sky. Ideally, model diagnostics should be screened using similar criteria. Within the GISS model we have found that all-sky and clear-sky AAOD do not differ greatly since the absorbing aerosols are assumed to be unaffected by relative humidity. Models that include aerosol mixing would probably have larger differences in AAOD for all-sky and clear-sky conditions.

The AAOD measurements include absorption by dust and "brown" or absorbing organic carbon. We have included all species in the model AAOD estimates, however we have not attempted to address shortcomings in dust simulations, and the models generally do not yet include significant absorption for organic carbon. However we have focused on regions where carbonaceous aerosols dominate over dust absorption. Furthermore, dust and absorbing organics absorb relatively less at longer wavelengths compared with BC. When we used the GISS model to consider the spectral dependence of the AAOD bias we found that the bias is generally independent of wavelength, suggesting BC is the primary source of bias.

A final difficulty is mismatch between dates for measurements and model emissions. We selected long-term measurements (one year or more) but the various measurements were taken from a variety of times. In regions where BC has been changing significantly, we may expect differing biases depending on the measurement and its date. The models generally used emissions for the 1990s. AERONET measurements are from 1996–2006, OMI from 2005–2007, IMPROVE from 1990s to 2002, EMEP for 2003–2004, many Asian surface concentration data are from 2006, and the SP2

ACPD
9, 15769–15825, 2009

measurements are for 2004–2008. Over the USA, there do not appear to be significant trends in the IMPROVE data for sites that have long-term surface concentration measurements (not shown). The other datasets are too short to observe significant trends. Some of the model bias in regions such as Southeast Asia, where BC may be increasing during the past 2 decades (Bond et al., 2007), may be due to a mismatch of emissions and measurement dates.

We may infer model underestimation of BC radiative forcing from the underestimation of AERONET AAOD. According to Table 9, the average model underestimates AAOD compared with AERONET by less than a factor of 2. The average AeroCom model BC radiative forcing is $+0.25\,\mathrm{Wm}^2$ (Schulz et al., 2006). If we assume that the radiative forcing is underestimated by the same amount as AAOD, then the average of AeroCom models would give a BC radiative forcing closer to $+0.5\,\mathrm{Wm}^{-2}$.

In spite of the uncertainties in models and measurements, our study has revealed some broad tendencies and biases in model BC simulations. Compared to column estimates of load and AAOD, the models generally underestimate BC. This bias is worst in biomass burning regions where the ratio of average model to retrieved is 0.4 to 0.7, remote regions (0.2 to 0.5) and Southeast Asia (0.6). To some extent the bias can be attributed to differing times for emissions and measurments in Southeast Asia, and to AERONET AAOD overestimation in remote regions. On the other hand, the models do not generally underestimate BC surface concentrations. At low-mid latitudes the models generally agree with the measurements near the surface, but overestimate the BC aloft over North America, especially in the mid-upper troposphere. At high latitudes many models underestimate BC in the lower and middle troposphere. The model-aircraft comparison suggests that models allow excessive vertical transport of BC, and may be lacking sufficient removal by precipitating clouds; they also probably lack sufficient low-level pole-ward transport. Unfortunately, enhancing BC rainout, especially at middle latitudes, is likely to diminish the BC available to travel pole-ward. Furthermore it will worsen the underestimate relative to AAOD.

This study suggests several future research directions to help close the gap be-

tween measurements and observations. To improve BC optical properties, models should include the effect of mixing with other species and increase refractive index as recommended by Bond and Bergstrom (2006) or approximate this effect by enhancing MABS for aged BC by 1.5 (Bond et al., 2006). Development of emissions inventories with size information and emission estimates of absorbing organic aerosols for model simulations should also be a priority. Models should include diagnostic simulators that screen in a manner like AERONET and OMI, e.g. only using sufficiently large AOD and in clear-sky daytime conditions. Important additional constraint would be provided by aircraft measurements over Eurasia, the oceans and the biomass burning regions. And long-term surface measurements co-located with AERONET stations, especially in remote and biomass burning regions, could help interpretation of model biases in these regions.

Acknowledgements. D. Koch was supported by NASA Radiation Sciences Program. Support from the Clean Air Task Force is acknowledged for support of SP2 measurements by the University of Hawaii. Ghan and Easter were funded by the US Department of Energy, Office of Science, Scientific Discovery through Advanced Computing (SciDAC) program and by the NASA Interdisciplinary Science Program under grant NNX07AI56G. The Pacific Northwest National Laboratory is operated for DOE by Battelle Memorial Institute under contract DE-AC06-76RLO 1830. The work with UIO-GCM was supported by the projects RegClim and AerOzClim, and supported by the Norwegian Research Council's program for Supercomputing through a grant of computer time. We acknowledge datasets for AERONET, available at http://aeronet.gsfc.nasa.gov; IMPROVE available from http://vista.cira.colostate.edu/IMPROVE; and EMEP from http://tarantula.nilu.no/projects/ccc. Analyses and visualizations of OMI AAOD were produced with the Giovanni online data system, developed and maintained by the NASA Goddard Earth Sciences (GES) Data and Information Services Center (DISC).

References

Acker, J. G. and G. Leptoukh: Online Analysis Enhances Use of NASA Earth Science Data", Eos, Trans. AGU, 88(2), p. 14 and 17, 2007.

Ackermann, I. J., Hass, H., Ebel, M. M., Binkowski, F. S., and Shankar, U.: Modal Aerosol Dynamics for Europe: Development and first applications, Atmos. Environ., 32, 2981–2999, 1998.
Andreae, M. O. and Merlet, P.: Emission of trace gases and aerosols from biomass burning, Global Biogeochem. Cy., 15, 955–966, 2001.
Andreae, M. O. and Gelencsér, A.: Black carbon or brown carbon? The nature of light-absorbing carbonaceous aerosols, Atmos. Chem. Phys., 6, 3131–3148, 2006, http://www.atmos-chem-phys.net/6/3131/2006/.
Balkanski, Y., Schulz, M., Claquin, T., Moulin, C., and Ginoux, P.: Global emissions of mineral aerosol: formulation and validation using satellite imagery, in: Emission of Atmospheric Trace Compounds, edited by: Granier, C., Artaxo, P., and Reeves, C. E., Kluwer, 253–282, 2003.
Barth, M. C., Rasch, P. J., Kiehl, J. T., Benkovitz, C. M., and Schwartz, S. E.: Sulfur chemistry in the NCAR CCM: Description, evaluation, features and sensitivity to aqueous chemistry, J. Geophys. Res., 106, 20311–20322, 2000.
Baumgardner, D., Kok, G., and Raga, G.: Warming of the Arctic lower stratosphere by light absorbing particles, Geophys. Res. Lett., 31(6), 1–4, 2004.
Bauer, S. E., Wright, D. L., Koch, D., Lewis, E. R., McGraw, R., Chang, L.-S., Schwartz, S. E., and Ruedy, R.: MATRIX (Multiconfiguration Aerosol TRacker of mIXing state): an aerosol microphysical module for global atmospheric models, Atmos. Chem. Phys., 8, 6003–6035, 2008, http://www.atmos-chem-phys.net/8/6003/2008/.
Bauer, S. E., Balkanski, Y., Schulz, M., Hauglustaine, D. A., and Dentener, F.: Global modeling of heterogeneous chemistry on mineral aerosol surfaces: In?uence on tropospheric ozone chemistry and comparison to observations, J. Geophys. Res. A., 109(D2), D02304, doi:10.1029/2003JD003868, 2004.
Berglen, T. F., Berntsen, T. K., Isaksen, I. S. A., and Sundet, J. K.: A global model of the coupled sulfur/oxidant chemistry in the troposphere: The sulfur cycle, J. Geophys. Res., 109, D19310, doi:10.1029/2003JD003948, 2004.
Bergstrom, R. W., Pilewskie, P., Russell, P. B., Redemann, J., Bond, T. C., Quinn, P. K., and Sierau, B.: Spectral absorption properties of atmospheric aerosols, Atmos. Chem. Phys., 7, 5937–5943, 2007, http://www.atmos-chem-phys.net/7/5937/2007/.
Berntsen, T. K., Fuglestvedt, J. S., Myhre, G., Stordal, F., and Berglen, T. F.: Abate-

ment of greenhouse gases: Does location matter?, Climatic Change, 27(4), 277–411, doi:10.1007/s10584-006-0433-4, 2006.
Bond, T. C. and R. W. Bergstrom: Light absorption by carbonaceous particles: An investigative review, Aerosol Sci. Tech., 40, 27–67, 2006.
Bond, T. C., Streets, D. G., Yarber, K. F., Nelson, S. M., Woo, J.-H., and Klimont, Z.: A technology-based global inventory of black and organic carbon emissions from combustion, J. Geophys. Res., 109, D14203, doi:10.1029/2003JD003697, 2004.
Bond T. C., Habib, G., and Bergstrom, R. W.: Limitations in the enhancement of visible light absorption due to mixing state, J. Geophys. Res., 111, D20211, doi:10.1029/2006JD007315, 2006.
Bond, T. C., E. Bhardwaj, R. Dong, R. Jogani, S. Jung, C. Roden, D. G. Streets, and N. M. Trautmann: Historical emissions of black and organic carbon aerosol from energy-related combustion, 1850–2000, Global Biogeochem. Cy., 21, GB2018, doi:10.1029/2006GB002840, 2007.
Boucher, O. and Anderson, T. L.: GCM assessment of the sensitivity of direct climate forcing by anthropogenic sulfate aerosols to aerosol size and chemistry, J. Geophys. Res., 100, 26 117–26 134, 1995.
Boucher, O., Pham, M., and Venkataraman, C.: Simulation of the atmospheric sulfur cycle in the Laboratoire de Meteorologie Dynamique General Circulation Model, Model description, model evaluation, and global and European budgets, Note scientifique de l'IPSL, 23, 2002.
Cakmur, R. V., Miller, R. L., Perlwitz, Ja., Koch, D., Geogdzhayev, I. V., Ginoux, P., Tegen, I., and Zender, C. S.: Constraining the global dust emission and load by minimizing the difference between the model and observations, J. Geophys. Res., 111, D06206, doi:10.1029/2004JD005550, 2006.
Chin, M., Ginoux, P., Kinne, S., Torres, O., Holben, B. N., Duncan, B. N., Martin, R. V., Logan, J. A., Higurashi, A., and Nakajima, T.: Tropospheric aerosol optical thickness from the GOCART model and comparisons with satellite and Sun photometer measurements, J. Atmos. Sci., 59(3), 461–483, 2002.
Chin, M., Rood, R. B., Lin, S.-J., Muller, J. F., and Thompson, A. M.: Atmospheric sulfur cycle in the global model GOCART: Model description and global properties, J. Geophys. Res., 105, 24 671–24 687, 2000.
Chow, J. C., Watson, J. G., Crow, D., Lowenthal, D. H., and Merrifield, T.: Comparison of IMPROVE and NIOSH carbon measurements, Aerosol Sci. Tech., 34, 23–34, 2001.

ACPD
9, 15769–15825, 2009

Claquin, T., Schulz, M., and Balkanski, Y.: Modeling the mineralogy of atmospheric dust, J. Geophys. Res., 104, 22243–22256, 1999.
Claquin, T., Schulz, M., Balkanski, Y., and Boucher, O.: The influence of mineral aerosol properties and column distribution on solar and infrared forcing by dust, Tellus B, 50, 491–505, 1998.
Clarke, A. D., McNaughton, C., Kapustin, V. N., Shinozuka, Y., Howell, S., Dibb, J., Zhou, J., Anderson, B., Brekhovskikh, V., Turner, H., and Pinkerton, M: Biomass burning and pollution aerosol over North America: Organic components and their influence on spectral optical properties and humidification response, J. Geophys. Res., 112, D12S18, doi:10.1029/2006JD007777, 2007.
Cofala, J., Amann, M., Klimont, Z., Kupiainen, K., and Höglund-Isaksson, L.: Scenarios of Global Anthropogenic Emissions of Air Pollutants and Methane Until 2030, Atmos. Environ., 41, 8486–8499, doi:10.1016/j.atmosenv.2007.07.010, 2007.
Cooke, W. F., Liousse, C., Cachier, H., and Feichter, J.: Construction of a 1x1 fossil fuel emission data set for carbonaceous aerosol and implementation and radiative impact in the ECHAM4 model, J. Geophys. Res., 104, 22137–22162, 1999.
Cooke, W. F. and Wilson, J. J. N.: A global black carbon aerosol model, J. Geophys. Res. A., 101(D14), 19395–19409, 1996.
Cozic, J., Verheggen, B., Mertes, S., Connolly, P., Bower, K., Petzold, A., Baltensperger, U., and Weingartner, E.: Scavenging of black carbon in mixed phase clouds at the high alpine site Jungfraujoch, Atmos. Chem. Phys., 7, 1797–1807, 2007, http://www.atmos-chem-phys.net/7/1797/2007/.
Crounse, J. D., DeCarlo, P. F., Blake, D. R., Emmons, L. K., Campos, T. L., Apel, E. C., Clarke, A. D., Weinheimer, A. J., McCabe, D. C., Yokelson, R. J., Jimenez, J. L., and Wennberg, P. O.: Biomass burning and urban air pollution over the Central Mexican Plateau, Atmos. Chem. Phys. Discuss., 9, 2699–2734, 2009, http://www.atmos-chem-phys-discuss.net/9/2699/2009/.
Dentener, F., Kinne, S., Bond, T., Boucher, O., Cofala, J., Generoso, S., Ginoux, P., Gong, S., Hoelzemann, J. J., Ito, A., Marelli, L., Penner, J. E., Putaud, J.-P., Textor, C., Schulz, M., van der Werf, G. R., and Wilson, J.: Emissions of primary aerosol and precursor gases in the years 2000 and 1750 prescribed data-sets for AeroCom, Atmos. Chem. Phys., 6, 4321–4344, 2006, http://www.atmos-chem-phys.net/6/4321/2006/.

Duncan, B. N., Martin, R. V., Staudt, A. C., Yevich, R., and Logan, J. A.: Interannual and Seasonal Variability of Biomass Burning Emissions Constrained by Satellite Observations, J. Geophys. Res., 108(D2), 4040, doi:10.1029/2002JD002378, 2003.

Dubovik, O., Smirnov, A., Holben, B. N., King, M. D., Kaufman, Y. J., Eck, T. F., and Slutsker, I.: Accuracy assessment of aerosol optical properties retrieval from AERONET sun and sky radiance measurements, J. Geophys. Res., 105, 9791–9806, 2000.

Dubovik, O. and King, M. D.: A flexible inversion algorithm for retrieval of aerosol optical properties from Sun and sky radiance measurements, J. Geophys. Res., 105, 20673–20696, 2000.

Dubovik, O., Holben, B., Eck, T. F., Smirnov, A., Kaufman, Y., King, M. D., Tanre, D., and Slutsker, I.: Variability of absorption and optical properties of key aerosol types observed in worldwide locations, J. Atmos. Sci., 59, 590–608, 2002.

Easter, R. C., Ghan, S. J., Zhang, Y., Saylor, R. D., Chapman, E. G., Laulainen, N. S., Abdul-Razzak, H., Leung, L. R., Bian, X., and Zaveri, R. A.: MIRAGE: Model description and evaluation of aerosols and trace gases, J. Geophys. Res., 109, D20210, doi:10.1029/2004JD004571, 2004.

Evangelista, H., Maldonado, J., Godoi, R. H. M., Pereira, E. B., Koch, D., Tanizaki-Fonseca, K., Van Grieken, R., Sampaio, M., Setzer, A., Alencar, A., and Gonçalves, S. C.: Sources and transport of urban and biomass burning aerosol black carbon at the south-west Atlantic coast, J. Atmos. Chem., 56, 225–238, doi:10.1007/s10874-006-9052-8, 2007.

Generoso, S., Bréon, F.-M., Balkanski, Y., Boucher, O., and Schulz, M.: Improving the seasonal cycle and interannual variations of biomass burning aerosol sources, Atmos. Chem. Phys., 3, 1211–1222, 2003, http://www.atmos-chem-phys.net/3/1211/2003/.

Ghan, S. J. and Easter, R. C.: Impact of cloud-borne aerosol representation on aerosol direct and indirect effects, Atmos. Chem. Phys., 6, 4163–4174, 2006, http://www.atmos-chem-phys.net/6/4163/2006/.

Ghan, S. J. and Zaveri, R. A.: Parameterization of optical properties for hydrated internally-mixed aerosol, J. Geophys. Res., 112, D10201, doi:10.1029/2006JD007927, 2007.

Ghan, S., Laulainen, N., Easter, R., Wagener, R., Nemesure, S., Chapman, E., Zhang, Y., and Leung, R.: Evaluation of aerosol direct radiative forcing in MIRAGE, J. Geophys. Res., 106, 5295–5316, 2001.

Giglio, L., van der Werf, G. R., Randerson, J. T., Collatz, G. J., and Kasibhatla, P.: Global

estimation of burned area using MODIS active fire observations, Atmos. Chem. Phys., 6, 957–974, 2006, http://www.atmos-chem-phys.net/6/957/2006/.

Ginoux, P., Chin, M., Tegen, I., Prospero, J., Holben, B., Dubovik, O., and Lin, S.-J.: Sources and global distributions of dust aerosols simulated with the GOCART model, J. Geophys. Res., 106, 20255–20273, 2001.

Gong, S. L., Barrie, L. A., Blanchet, J.-P., Salzen, K. V., Lohmann, U., Lesins, G., Spacek, L., Zhang, L. M., Girard, E., Lin, H., Leaitch, R., Leighton, H., Chylek, P., and Huang, P.: Canadian Aerosol Module: A size-segregated simulation of atmospheric aerosol processes for climate and air quality models 1. Module development, J. Geophys. Res., 108(D1), 4007, doi:10.1029/2001JD002002, 2003.

Grini, A., Myhre, G., Zender, C. S., and Isaksen, I. S. A.: Model simulations of dust sources and transport in the global atmosphere: Effects of soil erodibility and wind speed variability, J. Geophys. Res., 110, D02205, doi:10.1029/2004JD005037, 2005.

Grini, A., Zender, C. S., and Colarco, P. R.: Saltation Sandblasting behavior during mineral dust aerosol production, Geophys. Res. Lett., 29(18), 1868, doi:10.1029/2002GL015248, 2002.

Guelle, W., Balkanski, Y. J., Dibb, J. E., Schulz, M., and Dulac, F.: Wet deposition in a global size-dependent aerosol transport model, 2. Influence of the scavenging scheme on 210 Pb vertical pro?les, surface concentrations, and deposition, J. Geophys. Res., 103, 28875–28891, 1998a.

Guelle, W., Balkanski, Y. J., Schulz, M., Dulac, F., and Monfray, P.: Wet deposition in a global size-dependent aerosol transport model, 1. Comparison of a 1 year 210 Pb simulation with ground measurements, J. Geophys. Res., 103, 11429–11445, 1998b.

Guelle, W., Balkanski, Y. J., Schulz, M., Marticorena, B., Bergametti, G., Moulin, C., Arimoto, R., and Perry, K. D.: Modeling the atmospheric distribution of mineral aerosol: Comparison with ground measurements and satellite observations for yearly and synoptic timescales over the North Atlantic, J. Geophys. Res., 105, 1997–2012, 2000.

Guibert, S., Matthias, V., Schulz, M., Bsenberg, J., Eixmann, R., Mattis, I., Pappalardo, G.,Perrone, M. R. ,Spinelli, N., and Vaughan, G.: The vertical distribution of aerosol over Europe – Synthesis of one year of EARLINET aerosol lidar measurements and aerosol transport modeling with LMDzT–INCA, Atmos. Environ., 39, 2933–2943, 2005.

Hansen, J. E. and Travis, L. D.: Light scattering in planetary atmospheres, Space Sci. Rev., 16, 527–610, 1974.

Holben, B. N., Eck, T. F., Slutsker, I., et al.: AERONET – A federated instrument network and data archive for aerosol characterization, Remote Sens. Environ., 66, 1–16, 1998.
Howell, S. G., Clarke, A. D., Shinozuka, Y., Kapustin, V. N., McNaughton, C. S., Huebert, B. J., Doherty, S., and Anderson, T.: The Influence of relative humidity upon pollution and dust during ACE-Asia: size distributions and implications for optical properties, J. Geophys. Res., 111, D06205, doi:10.1029/2004JD005759, 2006.
Iversen, T.: On the atmospheric transport of pollution to the Arctic, Geophys. Res. Lett., 11, 457–460, 1984.
Iversen, T. and Seland, O.: A scheme for process-tagged SO4 and BC aerosols in NCAR CCM3: Validation and sensitivity to cloud processes, J. Geophys. Res. A., 107(D24), 4751, doi:10.1029/2001JD000885, 2002.
Kinne, S., Schulz, M., Textor, C., Guibert, S., Balkanski, Y., Bauer, S. E., Berntsen, T., Berglen, T. F., Boucher, O., Chin, M., Collins, W., Dentener, F., Diehl, T., Easter, R., Feichter, J., Fillmore, D., Ghan, S., Ginoux, P., Gong, S., Grini, A., Hendricks, J., Herzog, M., Horowitz, L., Isaksen, I., Iversen, T., Kirkevg, A., Kloster, S., Koch, D., Kristjansson, J. E., Krol, M., Lauer, A., Lamarque, J. F., Lesins, G., Liu, X., Lohmann, U., Montanaro, V., Myhre, G., Penner, J., Pitari, G., Reddy, S., Seland, O., Stier, P., Takemura, T., and Tie, X.: An AeroCom initial assessment – optical properties in aerosol component modules of global models, Atmos. Chem. Phys., 6, 1815–1834, 2006, http://www.atmos-chem-phys.net/6/1815/2006/.
Kirkevag, A. and Iversen, T.: Global direct radiative forcing by process-parameterized aerosol optical properties, J. Geophys. Res., 107(D20), 4433, doi:10.1029/2001JD000886, 2002.
Kirkevag, A., Iversen, T., Seland, Ø., and Kristjansson, J. E.: Revised schemes for aerosol optical parameters and cloud condensation nuclei in CCM-Oslo, in: Institute Report Series No. 28, Department of Geosciences, University of Oslo, Oslo, Norway, 2005.
Koch, D., Schmidt, G. A., and Field, C. V.: Sulfur, sea salt and radionuclide aerosols in GISS ModelE, J. Geophys. Res., 111, D06206, doi:10.1029/2004JD005550, 2006.
Koch, D., Bond, T., Streets, D., Unger, N., and van der Werf, G. R.: Global impacts of aerosols from particular source regions and sectors, J. Geophys. Res., 112, D02205, doi:10.1029/2005JD007024, 2007.
Lavoue, D., Liousse, C., Cachie, R. H., Stocks, B. J., and Goldammer, J. G.: Modeling of carbonaceous particles emitted by boreal and temperate wildfires at northern latitudes, J. Geophys. Res. A., 105(D22), 26871–26890, 2000.

Liu, X. and Penner, J. E.: Effect of Mt. Pinatubo H2SO4/H2O aerosol on ice nucleation in the upper troposphere using a global chemistry and transport model (IMPACT), J. Geophys. Res., 107(D12), doi:10.1029/2001JD000455, 2002.

McNaughton, C. S., Clarke, A. D., Kapustin, V., Shinozuka, Y., Howell, S. G., Anderson, B. E., Winstead, E., Dibb, J., Scheuer, E., Cohen, R. C., Wooldridge, P., Perring, A., Huey, L. G., Kim, S., Jimenez, J. L., Dunlea, E. J., DeCarlo, P. F., Wennberg, P. O., Crounse, J. D., Weinheimer, A. J., and Flocke, F.: Observations of heterogeneous reactions between Asian pollution and mineral dust over the Eastern North Pacific during INTEX-B, Atmos. Chem. Phys. Discuss., 9, 8469–8539, 2009, http://www.atmos-chem-phys-discuss.net/9/8469/2009/.

Metzger, S., Dentener, F., Krol, M., Jeuken, A., and Lelieveld, J.: Gas/aerosol partitioning II: global modeling results, J. Geophys. Res. A., 107(D16), 4313, doi:10.1029/2001JD001103, 2002a.

Metzger, S. M., Dentener, F. J., Lelieveld, J., and Pandis, S. N.: Gas/aerosol partitioning I: a computationally efficient model, J. Geophys. Res., 107(D16), 4312, doi:10.1029/2001JD001102, 2002b.

Miller, R. L., Cakmur, R. V., Perlwitz, Ja., Geogdzhayev, I. V., Ginoux, P., Kohfeld, K. E., Koch, D., Prigent, C., Ruedy, R., Schmidt, G. A., and Tegen, I.: Mineral dust aerosols in the NASA Goddard Institute for Space Sciences ModelE atmospheric general circulation model, J. Geophys. Res., 111, D06208, doi:10.1029/2005JD005796, 2006.

Moteki, N. and Kondo, Y.: Effects of mixing state on black carbon measurement by Laser-Induced Incandescence, Aerosol Sci. Tech., 41, 398–417, 2007.

Moteki, N., Kondo, Y., Miyazaki, Y., Takegawa, N., Komazaki, Y., Kurata, G., Shirai, T., Blake, D. R., Miyakawa, T., and Koike, M.: Evolution of mixing state of black carbon particles: Aircraft measurements over the western Pacific in March 2004, Geophys. Res. Lett., 34, L11803, doi:10.1029/2006GL028943, 2007.

Mueller, J.-F.: Geographical distribution and seasonal variation of surface emissions and deposition velocities of atmospheric trace gases, J. Geophys. Res., 97, 3787–3804, 1992.

Myhre, G., Berglen, T. F., Johnsrud, M., Hoyle, C. R., Berntsen, T. K., Christopher, S. A., Fahey, D. W., Isaksen, I. S. A., Jones, T. A., Kahn, R. A., Loeb, N., Quinn, P., Remer, L., Schwarz, J. P., and Yttri, K. E.: Modelled radiative forcing of the direct aerosol effect with multi-observation evaluation, Atmos. Chem. Phys., 9, 1365–1392, 2009, http://www.atmos-chem-phys.net/9/1365/2009/.

Myhre, G., Berntsen, T. K., Haywood, J. M., Sundet, J. K., Holben, B. N., Johnsrud, M., and Stordal, F.: Modelling the solar radiative impact of aerosols from biomass burning during the Southern African Regional Science Initiative (SAFARI-2000) experiment, J. Geophys. Res., 108, 8501, doi:10.1029/2002JD002313, 2003.

Nozawa, T. and Kurokawa, J.: Historical and future emissions of sulfur dioxide and black carbon for global and regional climate change studies, CGER-Report, CGER/NIES, Tsukuba, Japan, 2006.

Olivier, J. G. J., Bouwman, A. F., Maas, C. W. M. V. d., Berdowski, J. J. M., Veldt, C., Bloss, J. P. J., Vesschedijk, A. J. H., Zandveldt, P. Y. J., and Haverlag, J. L.: Description of EDGAR Version 2.0: A set of global emission inventories of greenhouse gases and ozone-depleting substances for all anthropogenic and most natural sources on a per country basis and on a 1×1 grid, pp. RIVM report 771060002/TNO-MEP report R96/119, Rijkinstituut voor Volksgezondheid en Milieu, Bilthoven, The Netherlands, 1996.

Olivier, J. G. J., Berdowski, J. J. M., Peters, J. A. H. W., Bakker, J., Visschedijk, A. J. H., and Bloos, J. P. J.: Applications of EDGAR including a description of EDGAR V3.0: reference database with trend data for 1970–1995, NRP Report, 410200 051, RIVM, Bilthoven, The Netherlands, 2002.

Penner, J. E., Eddleman, H., and Novakov, T.: Towards the development of a global inventory of black carbon emissions, Atmos. Environ., 27A, 1277–1295, 1993.

Pitari, G., Mancini, E., Rizi, V., and Shindell, D. T.: Impact of future climate and emissions changes on stratospheric aerosols and ozone, J. Atmos. Sci., 59, 414–440, 2002.

Pitari, G., Rizi, V., Ricciardulli, L., and Visconti, G.: High-speed civil transport impact: Role of sulfate, nitric acid trihydrate, and ice aerosol studied with a two-dimensional model including aerosol physics, J. Geophys. Res., 98, 23141–23164, 1993.

Ramanathan, V. and G. Carmichael: Global and regional climate changes due to black carbon, Nature Geoscience, 1, 221–227, 2008.

Rasch, P. J., Collins, W. D., and Eaton, B. E.: Understanding the INDOEX aerosol distributions with an aerosol assimilation, J. Geophys. Res., 106, 7337–7355, 2001.

Rasch, P. J., Feichter, J., Law, K., Mahowald, N., Penner, J., Benkovitz, C., Genthon, C., Giannakopoulos, C., Kasibhatla, P., Koch, D., Levy, H., Maki, T., Prather, M., Roberts, D. L., Roelofs, G.-J., Stevenson, D., Stockwell, Z., Taguchi, S., M., K., Chipperfield, M., Baldocchi, D., McMurry, P., Barrie, L., Balkanski, Y., Chatfield, R., Kjellstrom, E., Lawrence, M., Lee, H. N., Lelieveld, J., Noone, K. J., Seinfeld, J., Stenchikov, G., Schwartz, S., Walcek, C., and

Williamson, D. L.: A comparison of scavenging and deposition processes in global models: results from the WCRP Cambridge Workshop of 1995, Tellus B, 52, 1025–1056, 2000.

Reddy, M. S. and Boucher, O.: Global carbonaceous aerosol transport and assessment of radiative effects in the LMDZ GCM, J. Geophys. Res., 109(D14), D14202, doi:10.1029/2003JD004048, 2004.

Reddy, M. S., Boucher, O., Bellouin, N., Schulz, M., Balkanski, Y., Dufresne, J.-L., and Pham, M.: Estimates of global multicomponent aerosol optical depth and radiative forcing perturbation in the Laboratoire de Meteorologie Dynamique general circulation model, J. Geophys. Res., 110, D10S16, doi:10.1029/2004JD004757, 2005.

Sato, Mki., Hansen, J., Koch, D., Lacis, A., Ruedy, R., Dubovik, O., Holben, B., Chin, M., and Novakov, T.: Global atmospheric black carbon inferred from AERONET, P. Natl. Acad. Sci., 100, 6319–6324, doi:10.1073/pnas.0731897100, 2003.

Schulz, M., Textor, C., Kinne, S., Balkanski, Y., Bauer, S., Berntsen, T., Berglen, T., Boucher, O., Dentener, F., Guibert, S., Isaksen, I. S. A., Iversen, T., Koch, D., Kirkevåg, A., Liu, X., Montanaro, V., Myhre, G., Penner, J. E., Pitari, G., Reddy, S., Seland, Ø., Stier, P., and Takemura, T.: Radiative forcing by aerosols as derived from the AeroCom present-day and pre-industrial simulations, Atmos. Chem. Phys., 6, 5225–5246, 2006, http://www.atmos-chem-phys.net/6/5225/2006/.

Schuster, G. L., Dubovik, O., Holben, B. N., and Clothiaux, E. E.: Inferring black carbon content and specific absorption from Aerosol Robotic Network (AERONET) aerosol retrievals, J. Geophys. Res., 110, D10S17, doi:10.1029/2004JD004548, 2005.

Schwarz, J. P., Gao, R. S., Fahey, D. W., et al.: Single-particle measurements of midlatitude black carbon and lightscattering aerosols from the boundary layer to the lower stratosphere, J. Geophys. Res., 111, D16207, doi:10.1029/2006JD007076, 2006.

Schwarz, J. P., Spackman, J. R., Fahey, D. W., et al.: Coatings and their enhancement of black carbon light absorption in the tropical atmosphere, J. Geophys. Res., 113, D03203, doi:10.1029/2007JD009042, 2008.

Seland, Ø, Iversen, T., Kirkevåg, A., and Storelvmo, T.: On basic shortcomings of aerosol-climate interactions in atmospheric GCMs, Tellus, 60A, 459–491, doi:10.1111/j.1600-0870.2008.00318.x, 2008.

Shinozuka, Y., Clarke, A. D., Howell, S. G., Kapustin, V. N., McNaughton, C. S., Zhou, J., and Anderson, B. E.: Aircraft profils of aerosol microphysics and optical properties over North America: Aerosol optical depth and its association with $PM_{2.5}$ and water uptake, J. Geophys.

Res., 112, D12S20, doi:10.1029/2006JD007918, 2007.
Slowik, J. G., Cross, E. S., Han, J.-H., et al.: An intercomparison of instruments measuring black carbon content of soot particles, Aerosol Sci. Tech., 41, 295–314, 2007.
Smith, M. H. and Harrison, N. M.: The sea spray generation function, J. Aerosol Sci., 29, S189–S190, 1998.
Spackman, J. R., Schwarz, J. P., Gao, R. S., Watts, L. A., Thomson, D. S., Fahey, D. W., Holloway, J. S., de Gouw, J. A., Trainer, M., and Ryerson, T. B.: Empirical correlations between black carbon and carbon monoxide in the lower and middle troposphere, Geophys. Res. Lett., 35, L19816, doi:10.1029/2008GL035237, 2008.
Sprung, D., Jost, C., Reiner, T., Hansel, A., and Wisthaler, A.: Acetone and acetonitrile in the tropical Indian Ocean boundary layer and free troposphere: Aircraft-based intercomparison of AP-CIMS and PTR-MS measurements, J. Geophys. Res., 106(D22), 28511–28527, 2001.
Stier, P., Seinfeld, J. H., Kinne, S., and Boucher, O.: Aerosol absorption and radiative forcing, Atmos. Chem. Phys., 7, 5237–5261, 2007, http://www.atmos-chem-phys.net/7/5237/2007/.
Stier, P., Seinfeld, J. H., Kinne, S., Feichter, J., and Boucher, O.: Impact of nonabsorbing anthropogenic aerosols on clear-sky atmospheric absorption, J. Geophys. Res., 111(D18) D18201, doi:10.1029/2006JD007147, 2006.
Stier, P., Feichter, J., Kinne, S., Kloster, S., Vignati, E., Wilson, J., Ganzeveld, L., Tegen, I., Werner, M., Balkanski, Y., Schulz, M., Boucher, O., Minikin, A., and Petzold, A.: The aerosol-climate model ECHAM5-HAM, Atmos. Chem. Phys., 5, 1125–1156, 2005, http://www.atmos-chem-phys.net/5/1125/2005/.
Stohl, A.: Characteristics of atmospheric transport into the Arctic troposphere, J. Geophys. Res., 111, D11306, doi:10.1029/2005JD006888, 2006.
Takemura, T., Nozawa, T. T., Emori, S., Nakajima, T. Y., and Nakajima, T.: Simulation of climate response to aerosol direct and indirect effects with aerosol transport-radiation model, J. Geophys. Res., 110, D02202, doi:10.1029/2004JD005029, 2005.
Takemura, T., Nakajima, T., Dubovik, O., Holben, B. N., and Kinne, S.: Single-scattering albedo and radiative forcing of various aerosol species with a global three-dimensional model, J. Climate, 15(4), 333–352, 2002.
Takemura, T., Okamoto, H., Maruyama, Y., Numaguti, A., Higurashi, A., and Nakajima, T.: Global three-dimensional simulation of aerosoloptical thickness distribution of various origins, J. Geophys. Res., 105, 17853–17873, 2000.

Textor, C., Schulz, M., Guibert, S., Kinne, S., Balkanski, Y., Bauer, S., Berntsen, T., Berglen, T., Boucher, O., Chin, M., Dentener, F., Diehl, T., Easter, R., Feichter, H., Fillmore, D., Ghan, S., Ginoux, P., Gong, S., Grini, A., Hendricks, J., Horowitz, L., Huang, P., Isaksen, I., Iversen, I., Kloster, S., Koch, D., Kirkevåg, A., Kristjansson, J. E., Krol, M., Lauer, A., Lamarque, J. F., Liu, X., Montanaro, V., Myhre, G., Penner, J., Pitari, G., Reddy, S., Seland, Ø., Stier, P., Takemura, T., and Tie, X.: Analysis and quantification of the diversities of aerosol life cycles within AeroCom, Atmos. Chem. Phys., 6, 1777–1813, 2006, http://www.atmos-chem-phys.net/6/1777/2006/.

Textor, C., Schulz, M., Guibert, S., Kinne, S., Balkanski, Y., Bauer, S., Berntsen, T., Berglen, T., Boucher, O., Chin, M., Dentener, F., Diehl, T., Feichter, J., Fillmore, D., Ginoux, P., Gong, S., Grini, A., Hendricks, J., Horowitz, L., Huang, P., Isaksen, I. S. A., Iversen, T., Kloster, S., Koch, D., Kirkevåg, A., Kristjansson, J. E., Krol, M., Lauer, A., Lamarque, J. F., Liu, X., Montanaro, V., Myhre, G., Penner, J. E., Pitari, G., Reddy, M. S., Seland, Ø., Stier, P., Takemura, T., and Tie, X.: The effect of harmonized emissions on aerosol properties in global models – an AeroCom experiment, Atmos. Chem. Phys., 7, 4489–4501, 2007, http://www.atmos-chem-phys.net/7/4489/2007/.

Tie, X., Brasseur, G., Emmons, L., Horowitz, L., and Kinnison, D.: Effects of aerosols on tropospheric oxidants: A global model study, J. Geophys. Res., 106, 22 931–22 964, 2001.

Tie, X. X., Madronich, S., Walters, S., Edwards, D. P., Ginoux, P., Mahowald, N., Zhang, R. Y., Lou, C., and Brasseur, G.: Assessment of the global impact of aerosols on tropospheric oxidants, J. Geophys. Res. A., 110, D03204, doi:10.1029/2004JD005359, 2005.

van der Werf, G. R., Randerson, J. T., Collatz, G. J., and Giglio, L.: Carbon emissions from fires in tropical and subtropical ecosystems, Glob. Change Biol., 9, 547–562, 2003.

van der Werf, G. R., Randerson, J. T., Collatz, G. J., Giglio, L., Kasibhatla, P. S., Arellano, A. F., Olsen, S. C., and Kasischke, E. S.: Continental-scale partitioning of fire emissions during the 1997 to 2001 El Nino/La Nina period, Science, 303, 73–76, 2004.

van der Werf, G. R., Randerson, J. T., Giglio, L., Collatz, G. J., Kasibhatla, P. S., and Arellano Jr., A. F.: Interannual variability in global biomass burning emissions from 1997 to 2004, Atmos. Chem. Phys., 6, 3423–3441, 2006, http://www.atmos-chem-phys.net/6/3423/2006/.

Warneke, C., Bahreini, R., Brioude, J., Brock, C. A., de Gouw, J. A., Fahey, D. W., Froyd, K. D., Holloway, J. S., Middlebrook, A., Miller, L., Montzka, S., Murphy, D. M., Peischl, J., Ryerson, T. B., Schwarz, J. P., Spackman, J. R., and Veres, P.: Biomass burning in Siberia and Kaza-

khstan as an important source for haze over the Alaskan Arctic in April 2008, Geophys. Res. Lett., 36, L02813, doi:10.1029/2008GL036194, 2009.

Zhang, L., Gong, S.-L., Padro, J., and Barrie, L.: A Size-segregated Particle Dry Deposition Scheme for an Atmospheric Aerosol Module, Atmos. Environ., 35(3), 549–560, 2001.

Zhang, X. Y., Wang, Y. Q., Zhang, X. C., Guo, W., and Gong,S. L.: Carbonaceous aerosol composition over various regions of China during 2006, J. Geophys. Res., 113, D14111, doi:10.1029/2007JD009525, 2008.

Table 1. AeroCom model black carbon characteristics.

model	Energy Emis 1	BB Emis 1	Aging 2	BC lifetime days	Ice/snow removal 3	Diameter of emitted particle	BC density g cm^{-3}	Refractive index at 550 nm	MABS m^2 g^{-1}	References for aerosol module
GISS 99	B04	GFED	A	7.2	12%	0.08	1.6	1.56–0.5i	8.4	Koch et al. (2006, 2007); Miller et al. (2006)
ARQM 99	C99	L00, L96	I	6.7	T	0.1			4.1	Zhang et al. (2001); Gong et al. (2003)
CAM	C99	L00, L96	A							Gong et al. (2003)
DLR	CW96	CW96	I		5% accum, strat	0.08, 0.75 FF 0.02, 0.37 BB				Ackermann et al. (1998)
GOCART	C99	GFED, D03	A	6.6	T	0.078	1.0	1.75–0.45i	10.0	Chin et al. (2000, 2002); Ginoux et al. (2001)
SPRINTARS	NK06	NK06	BCOC		L	0.0695 FF, 0.1 others	1.25	1.75–0.44i	2.3	Takemura et al. (2000, 2002, 2005)
LOA B	B04	GFED	A	7.3	LI	0.1			8.0 #	Boucher and Anderson (1995); Boucher et al. (2002); Reddy and Boucher (2004); Guibert et al. (2005)
LSCE	G03	G03	A	7.5	L	0.14			3.5 (4.4 #)	Claquin et al. (1998, 1999); Guelle et al. (1998a,b, 2000); Smith and Harrison (1998); Balkanski et al. (2003); Bauer et al. (2004); Schulz et al. (2006)
MATCH	L96	L96	A		L	0.1				Barth et al. (2000); Rasch et al. (2000, 2001)
MOZGN	C99, O96	M92	A		L	0.1	1.0	1.75–0.44i	8.7	Tie et al. (2001, 2005)
MPIHAM	D06	D06	I #	4.9	S	0.069 (FF, BF) 0.172 (BB)	2.0	1.75–0.44i	7.7 #	Stier et al. (2005)
MIRAGE	C99	CW96, L00, O02	I		L	0.19, 0.025	1.7	1.9–0.6i	3, 6	Ghan et al. (2001); Easter et al. (2004); Ghan and Easter (2006)
TM5	D06	D06	A	5.7	20%	0.034	1.6	1.75–0.44i	4.3	Metzger et al. (2002a,b)
UIOCTM	C99	CW96	A	5.5	L	0.1 (FF), 0.295, 0.852 (BB)	1.0	1.55-0.44i	7.2 #	Grini et al. (2002, 2005); Myhre et al. (2003); Berglen et al. (2004); Berntsen et al. (2006)
UIOGCM 99	IPCC	IPCC	I #	5.5	none	0.0236–0.4	2.0	2.0-1.0i	10.5 #	Iversen and Seland (2002); Kirkevag and Iversen (2002); Kirkevag et al. (2005)
UMI	L96	P93	N	5.8	L	0.1452 (FF), 0.137 (BB)	1.5	1.80-0.5i	6.8 #	Liu and Penner (2002)
ULAQ 99	IPCC	IPCC	A	11.4	L	0.02–0.32	1.0	2.07–0.6i	7.5 #	Pitari et al. (2009, 2002)

1. BB=biomass burning; B04=Bond et al., 2004; C99=Cooke et al., 1999; L00=Lavoue et al., 2000; L96=Liouse et al., 1996; CW=Cooke and Wilson (1996); GFED=Van der Werf et al., (2003); NK06=Nozawa and Kurokawa (2006); G03=Generoso et al. (2003); R05=Reddy et al., (2005); D03=Duncan et al. (2003); D06=Dentener et al., (2006); M92=Mueller (1992); O96=Olivier et al. (1996); O02=Olivier (2002); IPCC=IPCC-TAR 2000; P93=Penner et al., (1993);
2. Aging as it affects particle solubility. A=aging with time; I=aging by coagulation and condensation; BCOC=BC assumed mixed with OC; N=none; # indicates that mixing/aging also affects particle optical properties;
3. T=Temp dependence, L=as liquid, LI=As liquid for in-cloud removal only; S=Stier et al. (2005); % is relative to water MABS=BC mass absorption coefficient at 550 nm, AAOD=aerosol absorption optical depth at 550 nm # Taken from Schulz et al. (2006).

ACPD
9, 15769–15825, 2009

Table 2. GISS model sensitivity studies.

Description	Emission Tg yr^{-1}	Burden mg m^{-2}	Lifetime, d	AAOD×100 550 nm
Standard run, see text	7.2 (4.4 energy, 2.8 biomass burning)	0.36	9.2	0.55
EDGAR emission	7.5	0.37	9.3	0.58
IIASA emission	8.1	0.41	9.5	0.60
GFED 1998	8.2	0.38	8.7	0.58
2×(Faster aging)	7.2	0.29	7.6	0.50
2×(Slower aging)	7.2	0.51	13	0.67
2×More ice-out	7.2	0.33	8.5	0.52
2×Less ice-out	7.2	0.38	9.8	0.57
Reff=0.1 μm	7.2	0.35	9.1	0.47
Reff=0.06 μm	7.2	0.36	9.3	0.70

ACPD
9, 15769–15825, 2009

Table 3. Average ratio between model and observed BC surface concentrations within regions for AeroCom models and GISS sensitivity studies. Number of measurements is given for each region. Bottom row is observed average concentration in ng m^{-3}. Regions defined as N Am (130 W to 70 W; 20 N to 55 N), Europe (15 W to 45 E; 30 N to 70 N), Asia (100 E to 160 E; 20 N to 70 N).

AeroCom models	N Am #26	Europe #16	Asia #23	Rest of World #12
GISS	0.81	0.65	0.43	2.4
CAM	1.6	2.2	0.40	1.8
GOCART	1.2	2.1	0.48	1.2
SPRINTARS	7.7	9.7	1.0	4.4
LOA	0.89	1.2	0.23	0.50
LSCE	0.61	3.0	0.43	0.81
MATCH	1.3	3.0	0.25	1.0
MOZGN	2.4	3.8	0.76	2.2
MPIHAM	1.5	0.73	0.56	0.44
TM5	1.8	1.0	0.76	1.2
UIOCTM	0.72	1.6	0.37	0.41
UIOGCM	0.88	2.9	0.53	1.7
UMI	0.81	4.8	0.65	1.0
ULAQ	0.75	3.0	0.82	2.2
Ave AeroCom	1.6	2.8	0.54	1.5
GISS sensitivity				
std	0.81	0.88	0.42	1.9
r=0.1	0.82	0.90	0.41	1.9
r=0.06	0.82	0.91	0.42	2.0
EDGAR	0.70	1.1	0.34	1.7
IIASA	0.70	0.86	0.50	1.9
BB1998	0.81	0.93	0.42	1.8
Lifex2	0.88	0.98	0.43	2.9
Life/2	0.78	0.80	0.38	1.5
Ice/2	0.83	0.93	0.41	2.1
Icex2	0.79	0.88	0.41	1.7
Observed (ng m^{-3})	290	1170	5880	750

ACPD
9, 15769–15825, 2009

Table 4. Average ratio of model to retrieved AERONET and OMI AAOD at 550 nm within regions for AeroCom models and GISS sensitivity studies. Number of measurements is given for AERONET. Annual and seasonal measurement values are given in last 5 rows. Regions defined as N Am (130 W to 70 W; 20 N to 55 N), Europe (15 W to 45 E; 30 N to 70 N), Asia (100 E to 160 E; 30 N to 70 N), S Am (85 W to 40 W; 34 S to 2 S), Afr (20 W to 45 E; 34 S to 2 S).

models	AAOD AER N Am #44	AAOD AER Eur #41	AAOD AER Asia #11	AAOD AER S Am #7	AAOD AER Afr #5	AAOD AER other #40	AAOD OMI N Am	AAOD OMI Eur	AAOD OMI Asia	AAOD OMI S Am	AAOD OMI Afr	AAOD OMI Rest of World
GISS	1.0	0.83	0.49	0.59	0.35	0.88	0.73	1.4	0.74	0.29	0.40	0.28
ARQM	0.79	0.36	0.30	0.42	0.25	0.44	0.50	0.61	0.40	0.22	0.23	0.19
SPRINTARS	1.4	0.48	0.44	1.8	1.2	0.64	0.76	0.69	0.59	0.83	1.3	0.28
LOA	0.57	0.56	0.42	0.44	0.70	0.44	0.32	0.95	0.44	0.25	0.48	0.18
LSCE	0.42	0.55	0.48	0.20	0.18	0.34	0.29	1.1	0.51	0.11	0.21	0.16
MOZGN	1.5	1.3	0.99	0.60	0.60	0.77	0.82	2.6	1.4	0.32	0.40	0.35
MPIHAM	0.39	0.21	0.29	0.43	0.35	0.21	0.21	0.29	0.32	0.22	0.35	0.082
MIRAGE	0.73	0.55	0.49	0.76	0.78	0.42	0.35	0.91	0.48	0.41	0.58	0.20
TM5	0.41	0.32	0.29	0.24	0.20	0.31	0.21	0.48	0.31	0.12	0.22	0.11
UIOCTM	0.62	0.67	0.46	1.1	0.61	0.57	0.37	1.1	0.53	0.57	0.54	0.19
UIOGCM	1.3	1.1	0.75	0.82	0.54	0.80	0.82	1.8	1.0	0.46	0.42	0.36
UMI	0.32	0.29	0.29	0.21	0.21	0.22	0.17	0.44	0.28	0.095	0.19	0.086
ULAQ	1.4	2.6	2.1	1.1	0.52	1.1	1.1	6.7	1.5	0.62	0.48	0.71
Ave	0.82	0.75	0.60	0.67	0.51	0.52	0.50	1.5	0.64	0.35	0.45	0.24
GISS sensitivity studies												
std	1.0	0.83	0.49	0.59	0.35	0.53	0.73	1.4	0.74	0.29	0.40	0.28
r=0.1	0.86	0.66	0.40	0.49	0.28	0.48	0.60	1.2	0.61	0.24	0.32	0.22
r=0.06	1.4	1.1	0.68	0.77	0.47	0.61	1.0	1.8	1.0	0.38	0.53	0.38
EDGAR	1.1	0.81	0.46	0.57	0.35	0.58	0.75	1.4	0.73	0.28	0.41	0.29
IIASA	1.2	0.85	0.57	0.59	0.36	0.55	0.82	1.5	0.90	0.29	0.41	0.32
BB1998	1.1	0.81	0.51	0.67	0.40	0.55	0.80	1.4	0.84	0.31	0.45	0.30
Lifex2	1.3	0.91	0.54	0.66	0.41	0.58	0.93	1.6	0.88	0.35	0.50	0.39
Life/2	0.93	0.73	0.46	0.58	0.33	0.52	0.65	1.3	0.67	0.28	0.37	0.23
Ice/2	1.1	0.83	0.51	0.62	0.36	0.52	0.81	1.5	0.79	0.29	0.41	0.31
Icex2	0.96	0.74	0.48	0.58	0.34	0.52	0.68	1.3	0.71	0.31	0.39	0.24
Std DJF	0.85	0.45	0.45	0.29	0.33	0.31	0.40	0.40	0.64	0.22	0.30	0.36
Std MAM	0.96	0.86	0.51	0.41	0.38	0.46	0.95	1.2	0.60	0.21	0.33	0.38
Std JJA	0.83	0.97	0.64	0.43	0.30	0.66	0.63	1.7	0.93	0.28	0.36	0.36
Std SON	1.2	0.64	0.56	0.51	0.34	0.40	0.63	0.80	0.71	0.20	0.57	0.38
Retrieved ×100												
AA	0.69	1.5	3.6	1.8	2.0	2.4	0.85	0.68	1.5	2.2	1.7	1.2
DJF	0.57	1.4	3.3	1.4	0.9	2.6	1.0	1.4	1.4	1.5	1.2	0.9
MAM	0.79	1.6	4.0	1.0	0.8	2.4	0.72	0.97	2.2	1.4	0.82	1.4
JJA	0.88	1.6	3.0	2.4	3.1	2.0	1.0	0.71	1.2	2.7	2.7	1.8
SON	0.57	1.6	3.0	3.1	3.9	2.2	0.95	1.0	1.4	4.7	1.4	1.1

ACPD
9, 15769–15825, 2009

Table 5. The average ratio of GISS model to AERONET within regions for 1000 nm and 550 nm.

Effective Radius, μm	AAOD Nam 44	AAOD Eur 41	AAOD Asia 11	AAOD S Am 7	AAOD Afr 5	AAOD Rest 21
1000 nm						
Std r=0.08	0.85	0.87	0.55	0.42	0.28	0.54
r=0.1	0.72	0.73	0.47	0.36	0.23	0.50
r=0.06	1.1	1.1	0.73	0.55	0.36	0.61
550 nm						
Std r=0.08	1.0	0.83	0.49	0.59	0.35	0.53
r=0.1	0.86	0.66	0.40	0.49	0.28	0.48
r=0.06	1.4	1.1	0.68	0.77	0.47	0.61

ACPD

9, 15769–15825, 2009

Table 6. Average ratio of model to retrieved AERONET BC column load using the Schuster et al. (2005) algorithm, within regions for AeroCom models and GISS sensitivity studies. Last row has average retrieved value in mg m^{-2}. Number of measurements is given for each region.

models	N Am 39	Eur 43	Asia 10	S Am 7	Afr 4	Rest 47
GISS	0.36	0.29	0.59	0.36	0.80	0.51
CAM	0.32	0.37	0.47	0.50	0.40	0.30
ARQM	0.47	0.45	0.54	0.45	0.40	0.41
DLR	0.58	0.87	0.44	0.55	1.1	0.44
SPRINTARS	1.2	1.3	0.91	0.63	2.2	0.65
GOCART	0.53	0.73	0.80	0.48	0.75	0.38
LOA	0.28	0.39	0.42	0.31	0.67	0.42
LSCE	0.34	0.58	0.81	0.27	0.32	0.36
MATCH	0.34	0.44	0.39	0.61	0.50	0.33
MOZGN	0.66	0.80	0.97	0.39	0.53	0.44
MPIHAM	0.22	0.19	0.45	0.34	0.38	0.20
MIRAGE	0.29	0.36	0.42	0.51	0.67	0.36
TM5	0.31	0.27	0.47	0.27	0.33	0.22
UIOCTM	0.28	0.44	0.48	0.46	0.82	0.52
UIOGCM	0.27	0.22	0.33	0.21	0.27	0.19
UMI	0.28	0.64	0.79	0.53	0.38	0.26
ULAQ	0.38	1.5	1.6	0.31	0.32	0.76
Ave	0.42	0.58	0.64	0.42	0.64	0.40
GISS sensitivity						
std	0.32	0.39	0.53	0.26	0.24	0.19
EDGAR	0.34	0.41	0.49	0.24	0.23	0.22
IIASA	0.37	0.42	0.64	0.25	0.24	0.23
BB1998	0.34	0.40	0.53	0.27	0.25	0.20
Lifex2	0.42	0.47	0.60	0.31	0.31	0.26
Life/2	0.28	0.34	0.47	0.25	0.21	0.16
Ice/2	0.35	0.39	0.54	0.27	0.24	0.20
Icex2	0.30	0.36	0.50	0.25	0.23	0.18
Retrieved						
	1.8	2.1	3.0	2.7	2.1	2.5

ACPD
9, 15769–15825, 2009

Table 7. Single Particle Soot Photometer (SP2) Measurements of Black Carbon Mass from Aircraft.

Fig.	Field Campaign[1]	Aircraft Platform	Investigator Group[2]	Dates	Number of Flights	Latitude Range	Longitude Range	Altitude Range (km)
9a	AVE Houston	NASA WB-57F	NOAA	10–12 Nov 2004	2	29–38° N	88–98° W	0–18.7
9b	CR-AVE	NASA WB-57F	NOAA	6–9 Feb 2006	3	1° S–10° N	79–85° W	0–19.2
9c	TC4	NASA WB-57F	NOAA	3–9 Aug 2007	5	2–12° N	80–92° W	0–18.6
9d	Spring ARCTAS	NASA DC-8	University of Tokyo	1–19 Apr 2008	3	34–60° N	118–167° W	0–12
9e	CARB	NASA DC-8 P3-B	University of Tokyo, Hawaii	18–26 Jun 2008	5+	33–54° N	105–127° W	0–13
10a	Spring ARCTAS	NASA DC-8	University of Tokyo	1–19 Apr 2008	7	60–89° N	60–168° W	0–12
10b	Spring ARCTAS	NASA P3-B	University of Hawaii			35–81° N	70–162° W	0–7.8
10c	ARCPAC	NOAA WP-3D	NOAA	12–21 Apr 2008	5	65–75° N	126–165° W	0–7.4
10d	Summer ARCTAS	NASA DC-8	University of Tokyo	29 Jun–13 Jul 2008	8	45–87° N	40–135° W	0–13
10e	Summer ARCTAS	NASA P3-B	University of Hawaii	28 Jun–12 Jul 2008	10	45–62° N	90–130° W	0–8.3

[1] AVE Houston: NASA Houston Aura Validation Experiment; CR-AVE: NASA Costa Rica Aura Validation Experiment; TC4: NASA Tropical Composition, Cloud, and Climate Coupling; ARCTAS: NASA Arctic Research of the Composition of the Troposphere from Aircraft and Satellites; CARB: NASA initiative in collaboration with California Air Resources Board; ARCPAC: NOAA Aerosol, Radiation, and Cloud Processes affecting Arctic Climate;

[2] NOAA: David Fahey, Ru-shan Gao, Joshua Schwarz, Ryan Spackman, Laurel Watts (Schwarz et al., 2006); University of Tokyo: Yutaka Kondo, Nobuhiro Moteki (Moteki and Kondo, 2007; Moteki et al., 2007); University of Hawaii: Antony Clarke, Cameron McNaughton, Steffen Freitag (Clarke et al., 2007; Howell et al., 2006; McNaughton et al., 2009; Shinozuka et al., 2007).

ACPD
9, 15769–15825, 2009

Table 8. Ratio of model to observed aircraft campaigns for south (Fig. 9a–c) and north (Fig. 10 using the median or background observed values where available). The lowest 2 model layers are not used.

model/observed	south	north
GISS	3.8	0.61
ARQM	14.9	1.5
CAM	15.4	0.20
GOCART	12.6	0.86
SPRINTARS	9.2	0.91
LOA	12.3	0.16
LSCE	19.0	0.43
MATCH	12.6	0.13
MOZART	13.8	1.0
MPI	5.3	0.08
MIRAGE	4.5	0.54
TM5	7.0	0.15
UIOCTM	6.6	0.17
UIOGCM	11.0	0.90
ULAQ	14.4	0.71
UMI	3.6	0.63
Ave	10.4	0.56

ACPD
9, 15769–15825, 2009

Table 9. Summary table: ratio of average model to observed/retrieved within regions, from Tables 3, 4 and 6.

Average model biases	N Am	Eur	Asia	S Am	Afr	Rest
Surface concentration	1.6	2.8	0.54	NA	NA	1.5
BC burden	0.42	0.58	0.64	0.42	0.64	0.40
AERONET AAOD	0.82	0.75	0.60	0.67	0.51	0.52
OMI AAOD	0.50	1.5	0.64	0.35	0.45	0.24

ACPD

9, 15769–15825, 2009

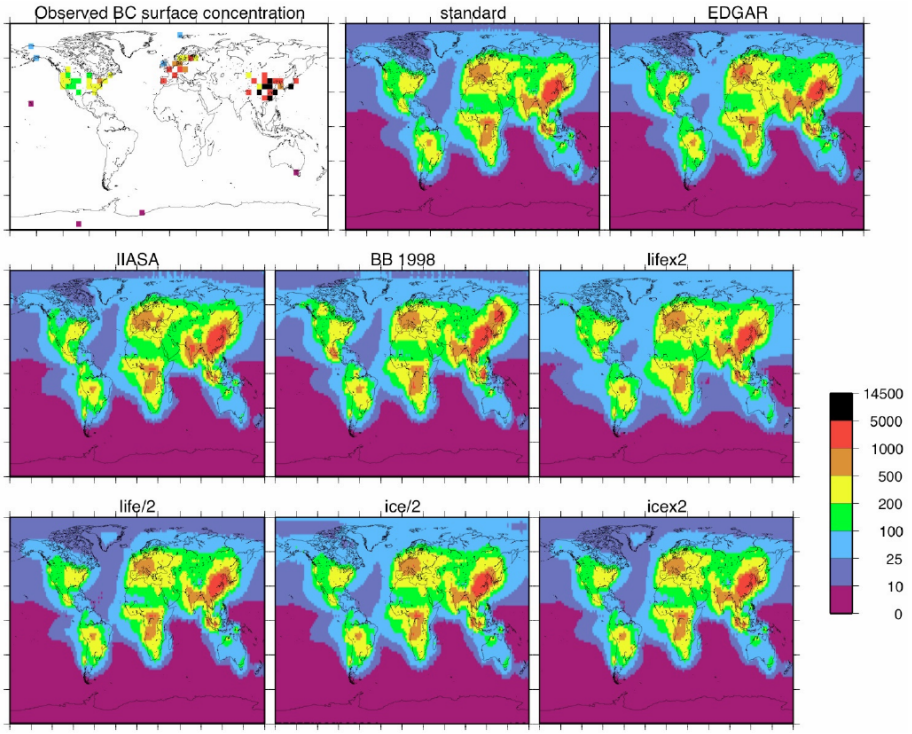

Fig. 1. Observed BC surface concentrations (upper left panel) and GISS sensitivity model results (annual mean; ng m^{-3}).

ACPD

9, 15769–15825, 2009

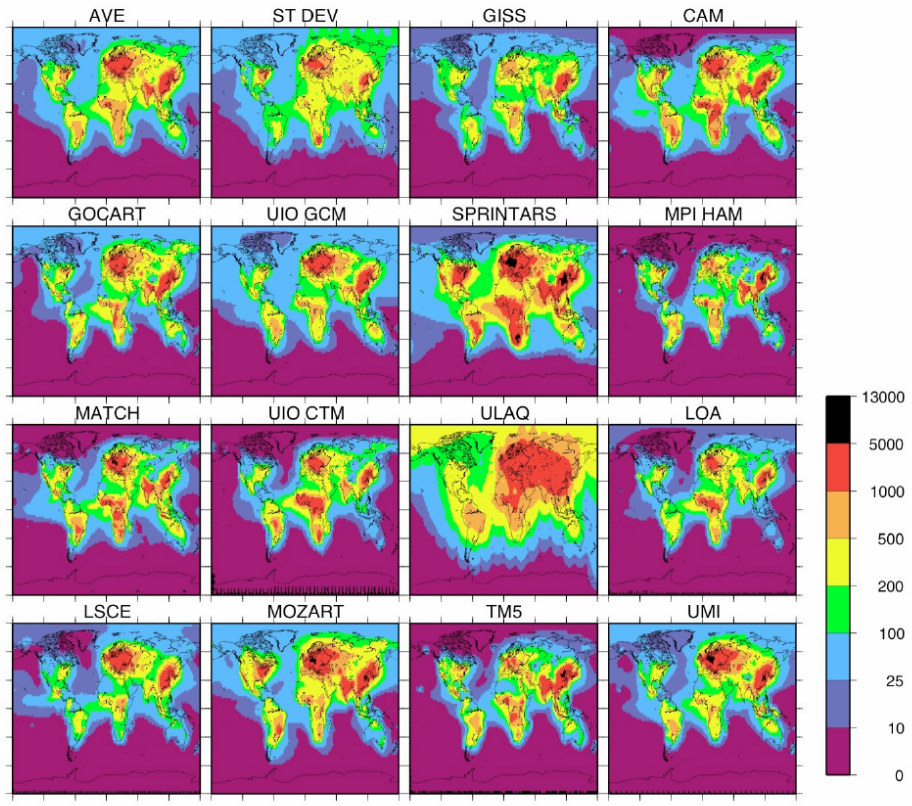

Fig. 2. AeroCom models' annual mean BC surface concentrations (ng m^{-3}). First panel shows average, second panel shows standard deviation of models.

ACPD

9, 15769–15825, 2009

Evaluation of black carbon estimations in global aerosol models

D. Koch et al.

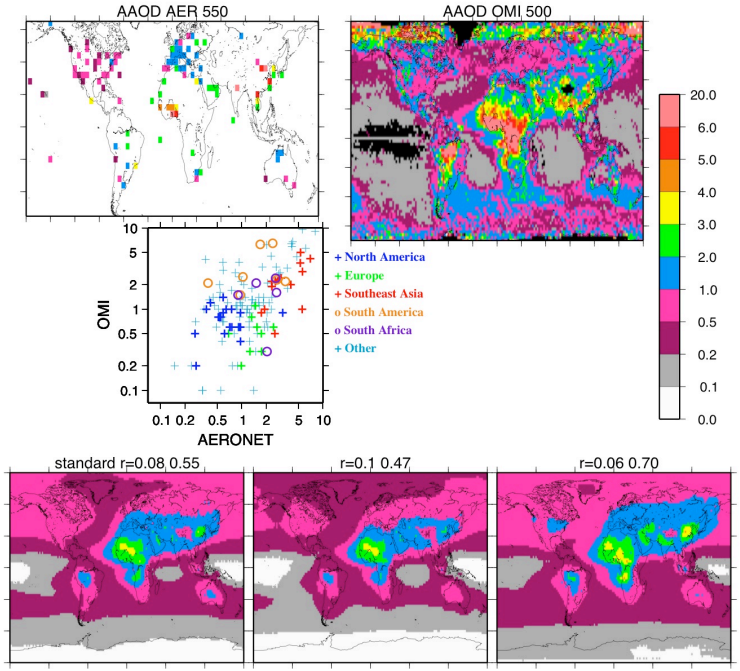

Fig. 3. Top: aerosol absorption optical depth, AAOD, (×100) from AERONET (at 550 nm; upper left), OMI (at 500 nm; upper right); middle: scatter plot comparing OMI and AERONET at AERONET sites; and bottom: GISS sensitivity studies for effective radius 0.08, 0.1, and 0.06 μm. The AERONET data are for 1996–2006, v2 level 2, annual averages for each year were used if >8 months were present, and monthly averages for >10 days of measurements. The values at 550 nm were determined using the 0.44 and 0.87 μm Angstrom parameters. The OMI retrieval is based on OMAERUVd.003 daily products from 2005–2007 that were obtained through and averaged using GIOVANNI (Acker and Leptoukh, 2007).

ACPD
9, 15769–15825, 2009

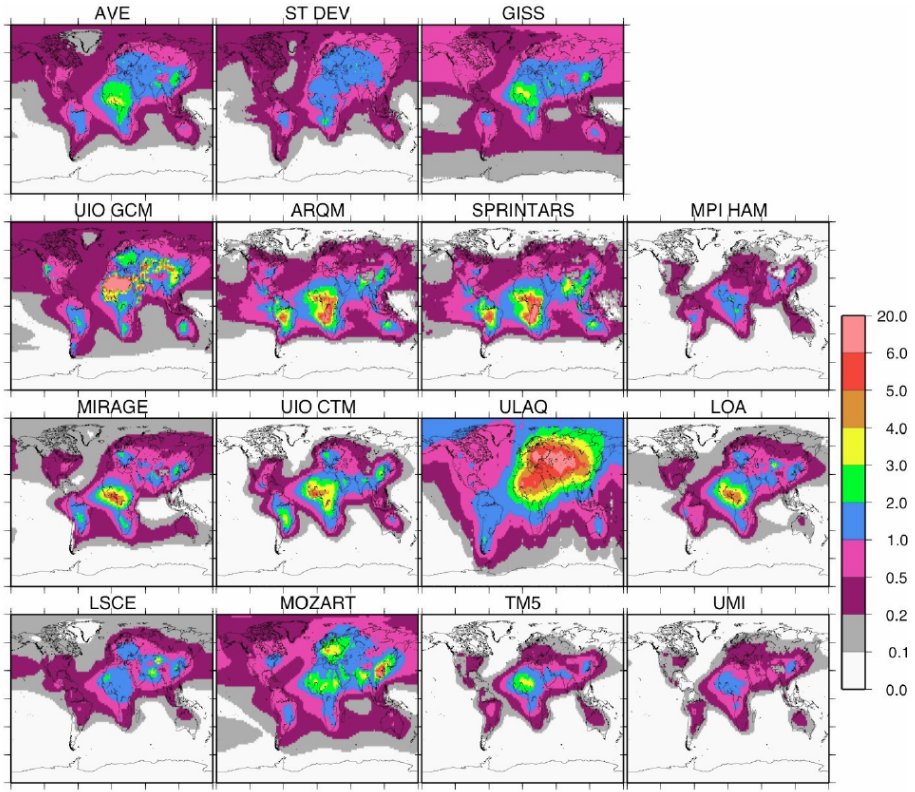

Fig. 4. Annual average AAOD (×100) for AeroCom models at 550 nm. First panel is average, second panel standard deviation.

ACPD

9, 15769–15825, 2009

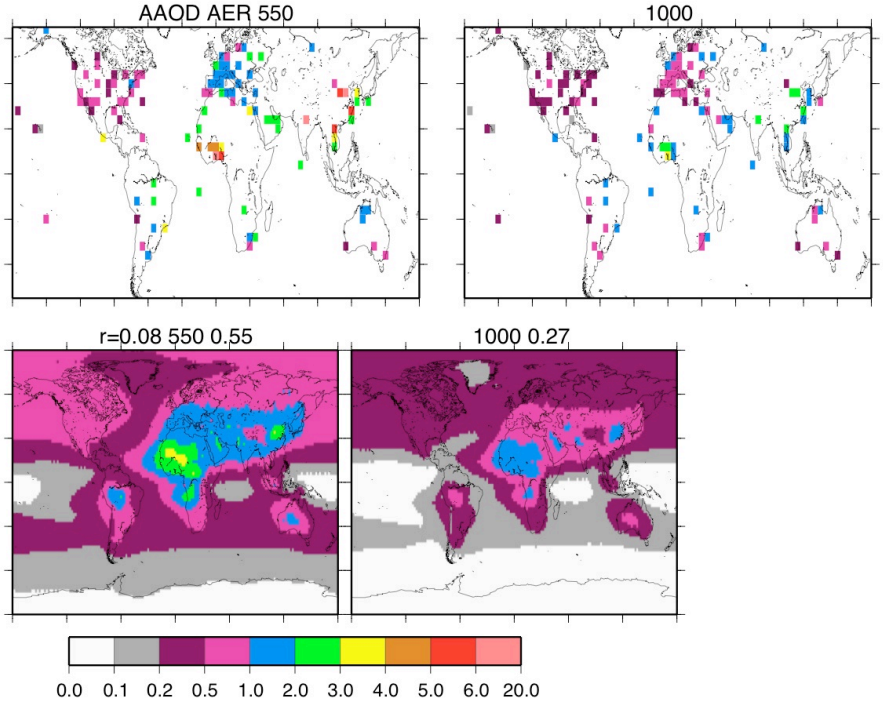

Fig. 5. Annual average AAOD (×100) at AERONET stations for 550 nm and 1000 nm (top left and right), and for the GISS model for 300–770 nm (bottom left) and 860–1250 nm (bottom right).

ACPD

9, 15769–15825, 2009

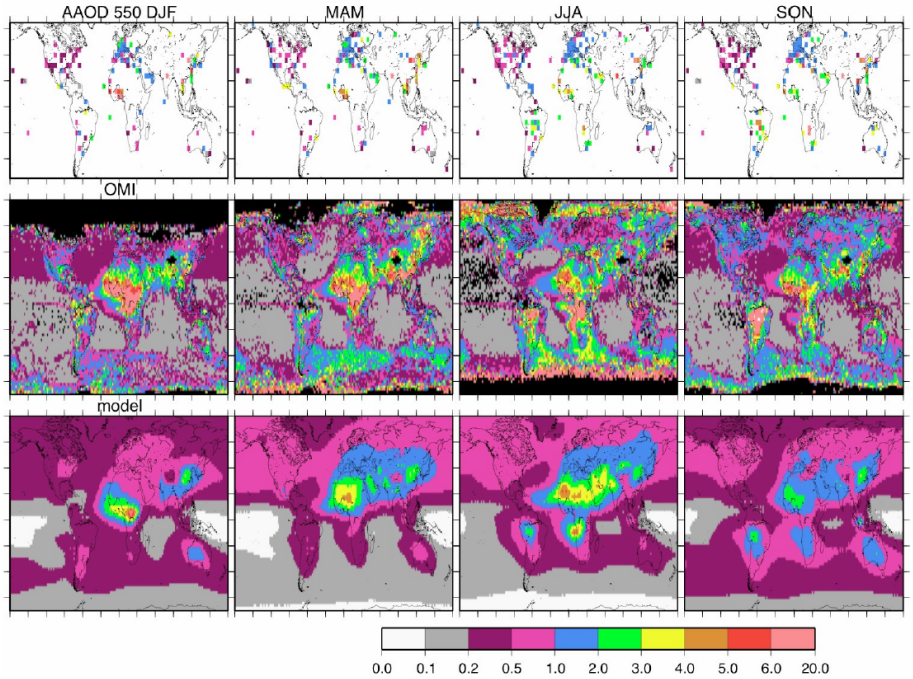

Fig. 6. Seasonal average AAOD (×100) for AERONET 550 nm (top), OMI 500 nm (middle), standard GISS model 550 nm (bottom).

ACPD

9, 15769–15825, 2009

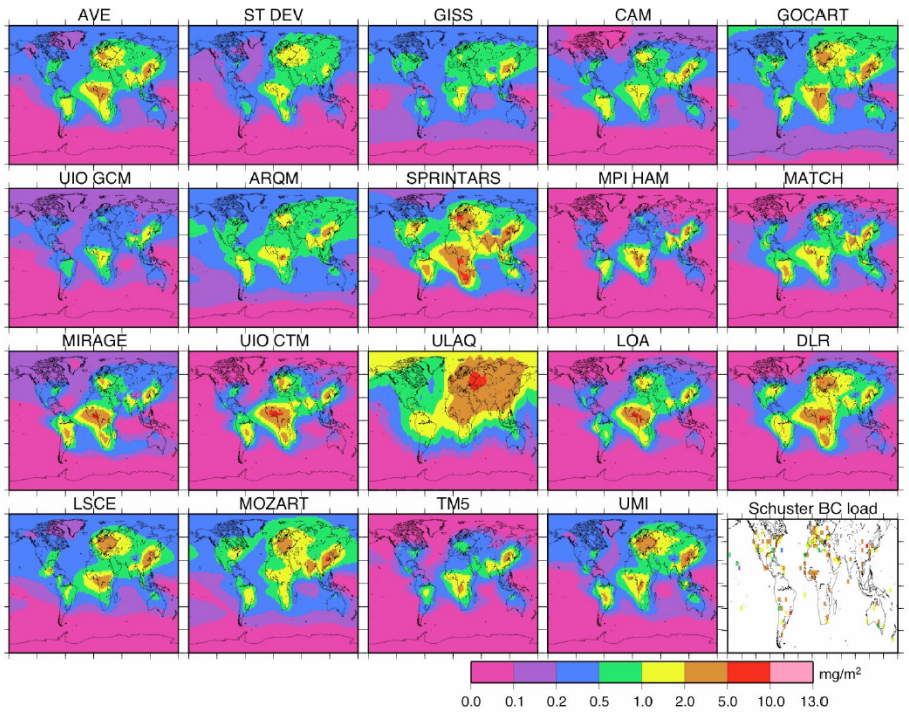

Fig. 7. Annual mean column BC load for AeroCom models, mg m^{-2}. The Schuster BC load is based on AERONET v2 level 1.5; annual averages require 12 months of data, data include all AERONET up to 2008.

ACPD

9, 15769–15825, 2009

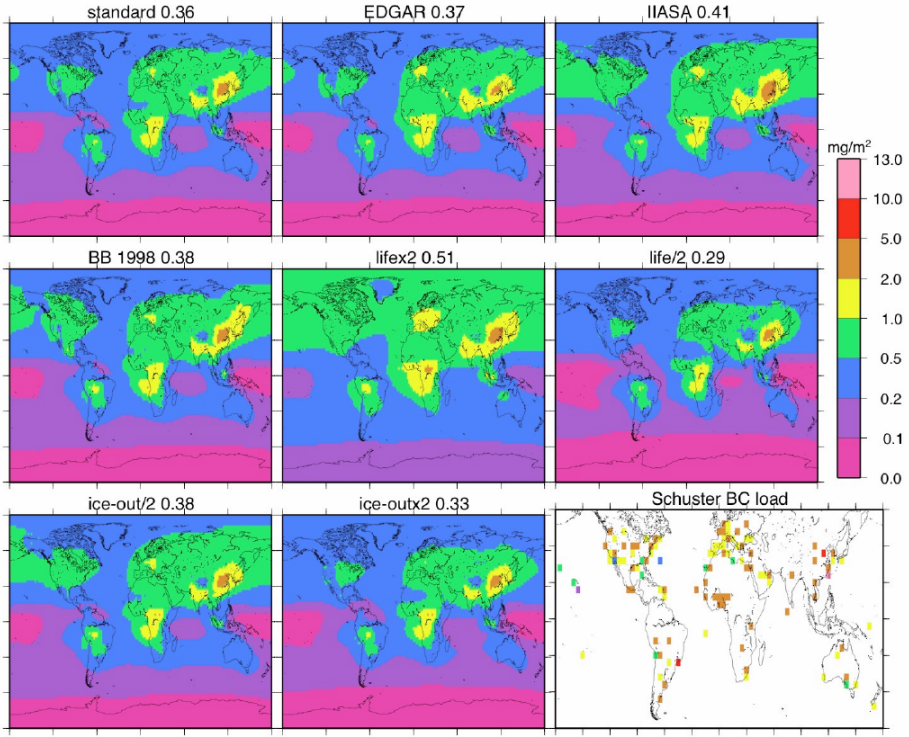

Fig. 8. Annual mean column BC load for GISS sensitivity simulations and the Schuster BC retrieval (see Fig. 7).

ACPD

9, 15769–15825, 2009

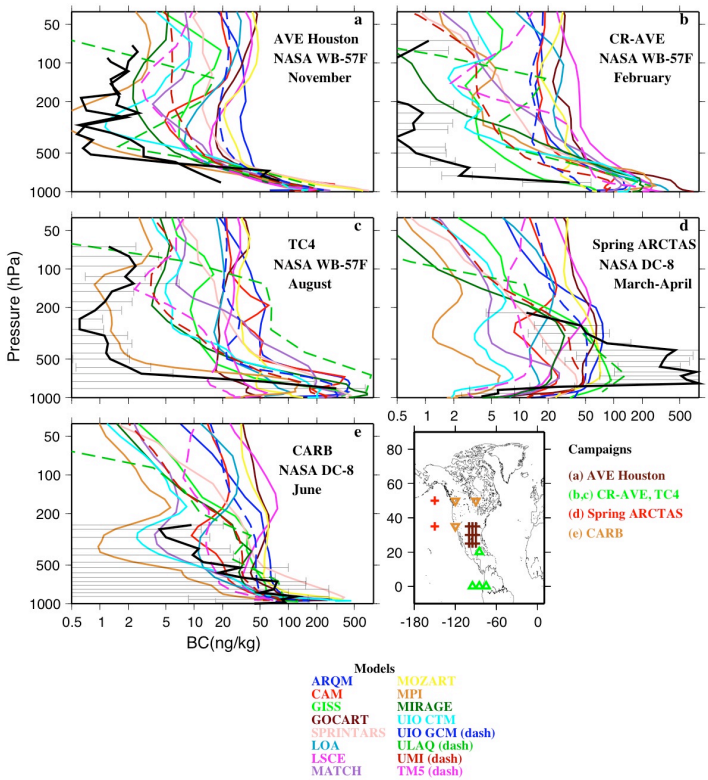

Fig. 9. Model profiles in approximate SP2 BC campaign locations in the tropics and midlatitudes, averaged over the points in the map (bottom). Observations (black curves) are average for the respective campaigns, with standard deviations where available. The Houston campaign has two profiles measured two different days. The markers in the map inset denote the location of model profiles in these comparisons with the aircraft measurements that are detailed in Table 7.

ACPD
9, 15769–15825, 2009

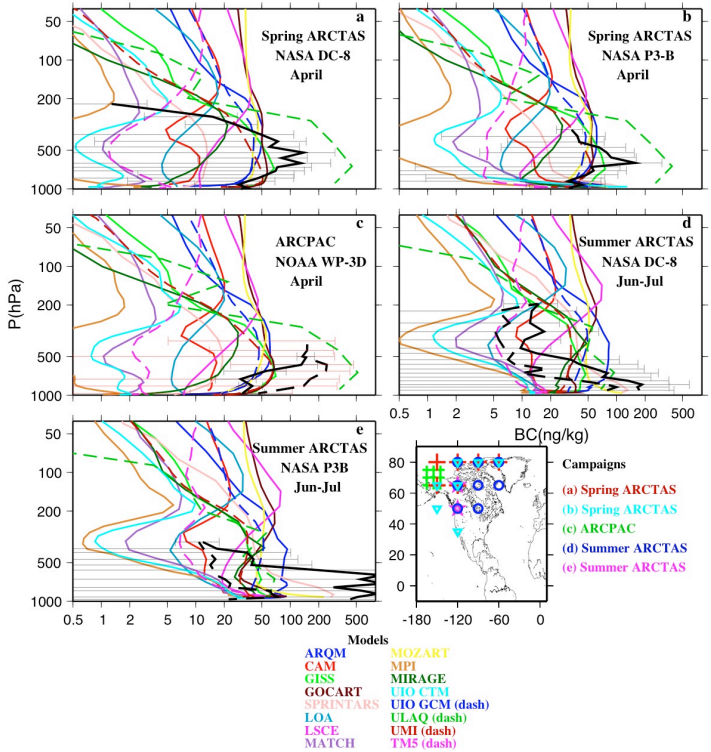

Fig. 10. Like Fig. 9 but for high latitude profiles. The ARCPAC campaign **(c)** has 2 profiles with 4 flights that probed long-range biomass burning plumes (dashed) and 1 flight that sampled aged Arctic air (solid). The summer campaign data **(d, e)** have both mean (solid) and median (dashed).

ACPD
9, 15769–15825, 2009